MASTER OF SCIENCE BY RESEARCH THESIS

Timing Pulsars with the Thousand Pulsar Array on MeerKAT

Author:
JASWANT JAYACUMAAR

Supervisor:
Dr. MICHAEL KEITH

A thesis submitted to the University of Manchester
for the degree of Master of Science by Research
in the

Department of Physics and Astronomy in the School of Natural Sciences
Faculty of Science and Engineering

2023

Contents

List of Figures

List of Tables

THE UNIVERSITY OF MANCHESTER

Abstract

Faculty of Science and Engineering

Department of Physics and Astronomy in the School of Natural Sciences

Master of Science by Research

Timing Pulsars with the Thousand Pulsar Array on MeerKAT

by JASWANT JAYACUMAAR

Pulsars are rotating neutron stars with rotational periods ranging from 1ms – 15s. This study employs the `TEMPO2` package to establish coherent timing solutions for regularly observed pulsars within the MeerTime Thousand-Pulsar-Array. The central focus of this dissertation is to explore variations in the pulsars' spin-down rate ($\dot{\nu}$) by analyzing the obtained timing residuals. Employing two distinct methodologies—Bayesian and fitwaves analysis, the latter being a novel addition to the study—we delve into the variations in $\dot{\nu}$. All timing observations originate from the Lovell telescope at the Jodrell Bank observatory (JBO) and the MeerKAT interferometer. By merging the JBO and MeerKAT data, a third dataset is created, and its contribution is assessed in estimating $\dot{\nu}$ variations through both methodologies. Comparative analysis aims to identify which dataset more effectively constrains $\dot{\nu}$ variations. The results reveal consistent $\dot{\nu}$ variations for the majority of pulsars between the two techniques. However, challenges arise in cases with limited observations or significant timing residual uncertainties along with irregularly sampled data, particularly impacting the fitwaves method. The creation of the third dataset has proven to be valuable. However, caution is advised in the utilization of data with high uncertainties, as it is preferable to exclude such data before conducting the analysis.

The document comprises 7,797 words.

Declaration of Authorship

I, JASWANT JAYACUMAAR, declare that this thesis titled, "Timing Pulsars with the Thousand Pulsar Array on MeerKAT" and the work presented in it are my own. I confirm that:

- This work was done wholly or mainly while in candidature for a research degree at this University.
- Where any part of this thesis has previously been submitted for a degree or any other qualification at this University or any other institution, this has been clearly stated.
- Where I have consulted the published work of others, this is always clearly attributed.
- Where I have quoted from the work of others, the source is always given. With the exception of such quotations, this thesis is entirely my own work.
- I have acknowledged all main sources of help.
- Where the thesis is based on work done by myself jointly with others, I have made clear exactly what was done by others and what I have contributed myself.

Copyright Statement

Acknowledgements

Foremost, I extend my sincere appreciation to my supervisor, Michael Keith, whose unwavering support, patience, and guidance were invaluable throughout my Master's. I am profoundly grateful for the opportunity to contribute to the JBCA Pulsar Group under his mentorship. My time in Manchester has been truly enriching, and I feel incredibly fortunate to have worked with such an exceptional supervisor and research group on exciting projects.

My heartfelt thanks go to the staff and postgrad students at JBCA, who made the proudest time of my life a happy one: Michael Keith, Patrick Weltevrede, Sotirios Sanidas, Anthony Holloway, Myfanwy Lloyd, James Turner, Avishek Basu, Thomas Rennie, James Stewart and Jonathan Wong. I extend my gratitude to the researchers at the Jodrell Bank Observatory and the MeerKAT interferometer for their efforts in processing the observational data.

Last but not least, I want to express my profound appreciation for the wonderful and supportive individuals who have played pivotal roles in my life, cheering me on in my research endeavors. In particular, my incredible parents, Sarada and Jayacumaar, my sister Sanjana, my grandma Santhakumari, and my friends Joshua, Sanjit, Anish, Sneha, Athira, Nandhini, Shravan, Vishak, and the members of EEB. I thank Adele and Jenny for being fantastic flatmates and making my time in Manchester truly memorable.

To everyone who has been part of this journey, thank you for the years of encouragement!

For my parents, my sister, my friends, my family, and everyone I love

–

Chapter 1

Introduction

1.1 Pulsars and Pulsar Timing

Neutron stars, remnants left behind by the supernova explosions of massive stars with masses ranging from 8 to 20 times that of the sun, represent the densest and most compact celestial bodies in the universe. These stellar remnants possess a solid crust initially characterized by temperatures in the range of 10^{11} to 10^{12} K. However, over the course of a few years, as energy is carried away by neutrinos, the temperature decreases substantially to 10^{6} K. During the collapse of the progenitor star, conservation of angular momentum, coupled with changes in radius, results in an increased spin rate and the establishment of a formidable magnetic field, often exceeding 10^{11} Gauss.

The intense magnetic fields of neutron stars function as strong particle accelerators. Typically, the misalignment of the dipole with the rotational axis generates beams of electromagnetic radiation emanating from the magnetic poles, transforming the neutron star into a cosmic lighthouse. These beams, manifesting as repeating pulses of radio signals, become detectable as the neutron star, now referred to as a pulsar, rotates and directs its emission along our line of sight.

Pulsars can be categorized as either recycled or non-recycled, a classification determined by their evolutionary background and the mechanism through which they attain their rotational speed. Recycled pulsars are commonly situated in binary systems, engaging in accretion processes with their companion stars, thereby acquiring angular momentum from the material they accrete. In contrast, non-recycled pulsars are those that have not undergone substantial mass transfer from a companion star. Pulsars, despite being inherently stable in their rotation, experience a gradual slowdown over

time due to the emission of radiation and energy loss. In the case of a pulsar exhibiting a spin frequency (ν), the spin frequency derivative ($\dot{\nu}$) serves to quantify the rate at which it spins down over time.

The braking index of a pulsar is a dimensionless parameter, relating the spin-down rate of a pulsar and its spin frequency. The braking index (n) is given by the equation 1.1:

$$n = \frac{\nu \ddot{\nu}}{\dot{\nu}^2} \tag{1.1}$$

where the $\ddot{\nu}$ is the second time derivative of the spin frequency.

Radio telescopes are equipped to capture the radio signals emitted by pulsars and record the precise time of arrival (ToA) of these pulses. The process of obtaining a pulse profile of a pulsar involves several steps. The recorded pulses are amplified at the receiver end to increase the signal strength and eventually, the signal-to-noise ratio, as the pulses travel interstellar distances and become weak by the time they reach our telescopes.

The pulses traverse through the interstellar medium (ISM) and get dispersed, causing a frequency-dependent delay. To resolve this, the signals are split into narrow frequency channels, and the time delay is applied using a dispersion formula to align the time of arrival and reverse the effect of dispersion - otherwise known as coherent de-dispersion (Hankins & Rickett, 1975). The power of the signals is added up to increase the signal-to-noise ratio of the pulse, as there is no attenuation. The time delay due to dispersion is given by equation 1.2:

$$\Delta t = 4.15 \left(\frac{\mathrm{DM}}{\mathrm{cm}^{-3} \cdot \mathrm{pc}} \right) \left[\left(\frac{\nu_1}{\mathrm{GHz}} \right)^{-2} - \left(\frac{\nu_2}{\mathrm{GHz}} \right)^{-2} \right] \mathrm{ms} \tag{1.2}$$

where Δt is time delay in milliseconds, DM is the dispersion measure in cm^{-3} pc, and ν_1 and ν_2 are the observing frequencies in GHz. The dispersion measure of pulsars quantifies the amount of dispersion a signal undergoes as it travels through the interstellar medium. The dispersion measure along the line of sight can be calculated from the above formula, as all the other parameters are known. The dispersion measure can also be represented by equation 1.3:

$$\mathrm{DM} = \int n_e \, dl \tag{1.3}$$

where n_e is the electron number density in cm^{-3}. Essentially, it denotes the cumulative density of free electrons along the observer's line of sight. Utilizing the dispersion measure and assuming a model for the distribution of galactic electron density, we can derive the distance to the pulsar. Another analogous term is the Rotation Measure (RM). The rotation measure of a pulsar is a measure of the amount of rotation of the polarization plane of the pulsar's radio waves due to the Faraday rotation effect as they propagate through the interstellar magnetic field. The rotation measure can also be represented by equation 1.4:

$$\mathrm{RM} = 0.81 \int n_e \mathbf{B} dl \tag{1.4}$$

where **B** is the vector magnetic field in microgauss (μG) and the rotation measure is in radians per square meter (rad m^{-2}). From RM, we can learn valuable information about the magnetic fields along the line of sight to the pulsar, which can help us understand the pulsar's environment, such as the interstellar medium and the magnetic properties of the pulsar itself. It provides insights into the distribution and strength of magnetic fields in the Galaxy, as well as aiding in studies of cosmic magnetism and the interstellar medium's properties (Han et al., 2018). Additionally, RM can be used to correct for the Faraday rotation effect, which is essential for accurately determining intrinsic properties of pulsars, such as their spin and magnetic field geometry.

Subsequently, the signal undergoes square-law detection, in which the power or intensity of the signal is directly proportional to the square of the electric field amplitude. Hence, it involves squaring the received signal. Mathematically, this is represented as $P_{out} = (V_{in})^2$, where V_{in} is the input voltage representing the pulsar signal and P_{out} is the output signal after squaring.

Later on, followed by a crucial procedure in pulse profile formation known as folding. During this stage, the pulse phase is determined on the basis of the pulse period and segmented into respective phase bins to accumulate signal intensity across multiple rotations. Ultimately, by summing the signal intensities from each phase bin, a pulse profile with a defined width is generated. This systematic process enhances the signal-to-noise ratio, facilitating the detection of the pulsar's periodicity.

Due to the gravitational influence exerted by a companion object such as a binary star or a planet orbiting the pulsar, or due to any internal mechanisms of the pulsar, the pulse profiles of each pulse differ over time. These fluctuations in the pulse shape of a pulsar observed over a period of time are

known as pulse profile variability. Examining pulse profile variability is important to understand the emission and internal mechanisms of a pulsar.

Thus far, we have explored the generation of the pulse profile and its variability. Following this, we proceed to determine the ToA from the pulse profile with its uncertainty. Section 2.1 provides an elucidation on the process of determining the Time of Arrival (ToA) from the pulse profile, encompassing details on its uncertainty. The assumption in pulsar timing is that the time of arrival of a pulse is treated as a singular point within the pulse profile. Ideally, it is chosen to be the point where the line of sight passes closest to the magnetic axis of the pulsar (Becker et al., 2018). Sections 2.2 and 2.3 offer insights into the data processing methodologies applied to the pulsar data at distinct observatories.

Subsequently, the ToA data undergo conversion into the pulse phase of emission within the barycentric reference frame of the solar system, considering the motion of Earth and other celestial bodies, as described in section 3.1. The measured pulse phase is then compared with a pre-existing pulsar model featuring a predicted pulse phase. The difference between the measured and predicted values gives rise to timing residuals in order to conduct pulsar timing analysis, as described in subsection 3.1.1. To refine the model, adjustments are made to known parameters, aiming to minimize these timing residuals. Despite parameter fitting, residual discrepancies persist, contributing to what is termed timing noise — unexplained variations in the timing of pulsar signals.

1.2 Timing Noise

Phenomena such as free precession (eg. Stairs et al. (2000)), the presence of binary and planetary companions (eg. Thorsett et al. (1993)), glitches (eg. Lyne et al. (2000)), and irregularities in spin-down, collectively known as timing noise, encompass various factors affecting pulsar behavior.

Glitches, abrupt increases in the pulsar's spin frequency (ν), manifest with spin-up rates ranging from 10^{-3} to 100 μHz. Following a glitch, there is a subsequent recovery phase during which the spin frequency is restored. Typically, glitches are quantified in terms of $\Delta\nu/\nu$, representing the difference in spin frequency. Although glitches are identified by sharp increases in timing residuals at specific epochs, timing noise is characterized by more rounded, wave-like structures occurring at multiple epochs. This study focuses primarily on utilizing timing noise for our analyses.

Pulsar timing noise, characterized by unexplained fluctuations in the arrival times of pulsar signals, is derived from a combination of intrinsic and extrinsic factors. Intrinsic factors include interactions with magnetic fields and the interior mechanisms of neutron stars, which remain incompletely understood. Extrinsic factors involve the interstellar medium (ISM) and companion objects. When pulsar signals traverse the ISM with varying density and properties, this results in delays or advances in pulse arrival times. Companions, whether stars in binary systems or planets in orbit, exert gravitational influences leading to observable timing variations.

The timing noise exhibits characteristics of both red and white noise, depending on the specific features of the timing variations. Red noise refers to long baseline changes in ToAs that are quasi-periodic in nature and characterized by low-frequency variations. White noise is characterized by random and uncorrelated fluctuations, such that they exhibit a Gaussian distribution around zero. To mitigate the effects of long-term correlations or variations such as red noise, the ToAs are adjusted through a procedure known as whitening. In this process, the ToAs are adjusted by fitting the red noise, resulting in whitened ToAs. This process helps in simplifying the data analysis and isolating specific features of interest by reducing the impact of long-term correlated variations.

The study by Hobbs et al. (2010) has determined that timing noise is a prevalent occurrence across all pulsars, and its manifestation is not attributable to observation systems or data processing methods. Furthermore, the research establishes that the nature of timing noise exhibits variability in structure based on the span of the observed data; notably, an increase in quasi-periodic features is observed as more data is accumulated. It also notes an inverse correlation between the timing noise and the characteristic age of the pulsar. Particularly for pulsars with a characteristic age below 10^5 years, it is suggested that the observed timing noise is explained as a recovery from preceding glitch events.

1.3 Thousand-Pulsar Array Programme

The Thousand-Pulsar Array (TPA) programme is a part of the 'MeerTime' survey project on the MeerKAT Telescope (Johnston et al., 2020). The objectives of the programme are to obtain:

1. High-fidelity pulse profiles for 1000+ non-recycled pulsars with polarisation properties.
2. More than 1000 single pulses from 500 bright pulsars to conduct standard single-pulse analysis.
3. Observation of 500 bright pulsars over multiple epochs.

The scientific goals of the programme are to determine the geometry of pulsars, the nature and location of the radio emission, the relation between the magnetosphere and the crust and core of the star. In addition to this, properties of the interstellar medium can be recovered by measuring the dispersion of the pulsar signals as it travels through the ISM.

MeerKAT is a radio interferometer with 64 antennas located in the Northern Cape of South Africa. It observes with a 'tied-array beam' and a wide bandwidth, that makes it suitable for pulsar observations with less statistical noise on a pulse profile. By combining the signals from multiple antennas, a single tied-array beam is formed to increase the sensitivity of the interferometer and to obtain observations with a high signal-to-noise ratio (S/N).

Dispersion measure (DM) and rotation measure (RM) yields information about the total electron density and the integrated magnetic field strength along the line of sight, respectively. The wide bandwidth of MeerKAT is very useful in obtaining information on DM and RM.

Forming $\mathcal{N}$ sub arrays reduces the sensitivity of the telescope by a factor of $\mathcal{N}$, and the observing time increases to $\mathcal{N}$-squared to get the same sensitivity. Most of our observations are dominated by the pulse-to-pulse variation, not by the S/N, or the optimal observing time is so short (i.e. < 60s) that overheads dominate. In this regime, it might be more efficient to sacrifice some sensitivity to observe multiple pulsars at the same time with multiple arrays.

Two legacy datasets are produced from the TPA programme. The first dataset contains the polarimetric pulse profiles of 1000+ pulsars obtained with a high S/N. This dataset can be used to measure the standard parameters such as DM, RM and pulse widths (Posselt et al., 2021). In addition to this, single pulse data from 500 bright pulsars are obtained to understand the mechanisms behind pulsar magnetosphere and radio emission (Johnston et al., 2020). However, more than 500 pulsars were observed since the start of the project and the single pulses were recorded for 1198 pulsars recently (Song et al., 2023). The second dataset contains observations of 500 bright pulsars over multiple epochs, used to conduct pulsar timing and emission variability studies (Song et al., 2021). To obtain this dataset, MeerKAT uses two 32-dish sub-arrays and considers it to be the most efficient way.

1.4 Variations in Spin-down rate and Bayesian Inference

Extensive research has been conducted on the variations in $\dot{\nu}$ through three distinct studies in the past. The initial investigation, led by Hobbs et al. (2004), aimed to derive proper motions and braking indices for pulsars utilizing the FITWAVES methodology (outlined in section 3.2.2). Notably, this study underscored that the obtained braking indices are affected by timing noise, and are not reflective of the intrinsic physics governing pulsar braking mechanisms.

The second study, carried out by Lyne et al. (2010) and extended in Shaw et al. (2022), focused on discerning correlations between $\dot{\nu}$ variations and changes in pulse shape. Meanwhile, the third study, conducted by Brook et al. (2015), concentrated on identifying correlations between the emission and rotation of a pulsar through a map of pulse profile variability. Both the second and third studies employed a non-parametric Gaussian process modeling approach, developed by Brook et al. (2015) and Brook et al. (2013). It is important to note that this modeling method does not perform optimally with irregularly sampled data.

Bayesian inference has found application in various facets of pulsar timing research. In the work conducted by Lentati et al. (2013a), a Bayesian approach was employed to estimate the spectral properties of an isotropic gravitational wave background (GWB). In another study by Lentati in the same year (Lentati et al., 2013b), a novel Bayesian technique known as `TEMPONEST` was introduced for analyzing the timing model. This approach incorporated additional stochastic parameters to investigate red noise and variations in dispersion measure (DM).

The work by Vigeland & Vallisneri (2014) employed a fully non-linear Bayesian approach to derive pulsar parameters and explore the statistical properties of noise originating from both the pulsar and the detector. In the research conducted by Niţ u et al. (2022), the same Bayesian technique slated for use in this study was applied to search for planetary companions around pulsars within the Jodrell Bank database.

Given the limitations encountered in previous studies when measuring $\dot{\nu}$ variations using the methods employed, primarily stemming from the challenges posed by irregularly sampled data, we have opted to employ the most recent Bayesian inference technique as mentioned in Keith et al. (2022). This approach will be applied to analyze the timing models of pulsars and extract information regarding $\dot{\nu}$ variations. Additionally, we utilize the `FITWAVES` methodology for conducting a comparative

analysis of the obtained results. Comprehensive descriptions of both the Bayesian and `FITWAVES` methodologies can be found in subsections 3.2.1 and 3.2.2, respectively.

Chapter 2

Observations

2.1 Time of Arrival (ToA) Determination

The precision of the Time of Arrival (ToA) is determined by the width and the S/N of the beam, given by the radiometer equation (Lorimer & Kramer, 2004):

$$\frac{S}{N} = \frac{S_\nu G \sqrt{n_p t_{obs} \Delta\nu}}{T_{sys}} \sqrt{\frac{P - W}{W}} \tag{2.1}$$

where S_ν is the pulsar's mean flux density (Jy), G is the gain of the telescope (K/Jy), n_p is the summation of number of polarizations, t is the observing integration time (s), $\Delta\nu$ is the observing bandwidth, T_{sys} is the system temperature (K), P and W are pulse period (s) and pulse width (s).

In elucidating the constituents of the formula, an explanation of each term is provided. Mean flux density denotes the average intensity of radiation received from the pulsar over a specific time. The gain of a telescope is defined as the ratio of the radiation intensity emitted per unit solid angle in a specific direction by the antenna, relative to that of an isotropic antenna. The pulse period refers to the time interval between successive pulses of radiation from a pulsar. The system temperature refers to the total noise temperature produced by the observing systems. The system temperature can be represented by equation 2.2:

$$T_{sys} = T_{rec} + T_{spillover} + T_{sky} \tag{2.2}$$

where T_{rec} is the noise temperature associated with the radio receiver, $T_{spillover}$ is the noise temperature due to unwanted ground sources in the telescope's field of view, and T_{sky} is the noise temperature due to the cosmic microwave background (CMB) and other celestial objects in the sky.

To obtain the ToA from the pulse profile, identify a reference point within the pulse profile associated with a specific feature, such as the peak or leading edge of the pulse. Subsequently, establish a time reference point, typically corresponding to the start of the observation or a known reference time. Measure the time difference (Δt) between the reference time and the selected reference point on the pulse profile. Ultimately, the ToA is determined using the following equation:

$$\text{ToA} = \text{Reference Time} + \Delta t \tag{2.3}$$

Though this provides a broad overview, a more comprehensive discussion on determining the ToA and other implemented algorithms can be found in van Straten et al. (2012).

For every ToA determination, an associated uncertainty is established, originating from a combination of intrinsic and instrumental factors. The uncertainty in ToA, denoted as σ_{TOA}, is quantified using the following equation (Lorimer & Kramer, 2004):

$$\sigma_{TOA} \simeq \frac{W}{S/N} \propto \frac{S_{sys}}{\sqrt{t_{obs}\Delta\nu}} \times \frac{P^{3/2}}{S_\nu} \tag{2.4}$$

While this serves as a general equation, a comprehensive explanation of ToA determination and uncertainty measurements can be found in Section 2 and Appendix A of Taylor (1992), respectively.

The software applications employed in this study, namely `TEMPO2` (section 3.1), `RUN-ENTERPRISE` (subsection 3.2.1), and `FITWAVES` (subsection 3.2.2), incorporate their respective built-in algorithms for standard error analysis to determine uncertainties.

2.2 Jodrell Bank Specifications

The pulsars investigated in this research were observed using the 76-m Lovell telescope at the Jodrell Bank Observatory in Macclesfield, United Kingdom. The observations were conducted at a center frequency of 1520 MHz with a bandwidth of 400 MHz, and the data were recorded utilizing a digital filterbank (DFB), as outlined in Manchester et al. (2013). The data were folded on to 1024 bins per

pulse period, along with subintegations of 10 seconds and 768 frequency channels. A median filtering algorithm was applied to eliminate the majority of radio frequency interference (RFI) (Basu et al., 2021), and any remaining interference was manually removed from the affected channels or subintegrations. Using the technique detailed in Hotan et al. (2004), the DFB observations were recorded in the `PSRFITS` format, and subsequent data reduction and Time of Arrival (ToA) generation were carried out using the `PSRCHIVE` software. Additional details regarding the backend systems employed in this study can be found in the work of Shemar & Lyne (1996).

2.3 MeerKAT Specifications

The observations used for the pulsar timing in this work were collected using the MeerKAT radio telescope. MeerKAT is a radio interferometer with an array of $\mathcal{N}$ antannae. Therefore, for a coherently phased array, the sensitivity will increase by $\mathcal{N}$ times, and for an incoherently phased array, the sensitivity will increase by $\sqrt{\mathcal{N}}$ times in the standard radiometer equation given above. MeerKAT employs the tied-array beam technique to achieve real-time coherence by synchronizing the phase and amplitude of signals from all antennas. This process enhances sensitivity and resolution, contributing to the telescope's observational capabilities.

The observations were conducted at various epochs using the MeerKAT telescope at *L*-band, centered at a frequency of 1284 MHz with a bandwidth of 856 MHz and employing two orthogonal linear polarisations. MeerKAT is characterized by a system temperature of 18.15 K and a gain of 2.8 K/Jy (Bailes et al., 2020). The data underwent coherent de-dispersion to mitigate interstellar effects, utilizing dispersion measurement data before being folded. The Time of Arrival (ToA) were generated by using the `PSRCHIVE` software, as detailed in section 2.2.

2.4 Observational Data Integrity

In both MeerKAT and Lovell observations, the Time of Arrival (ToA) is calculated by employing a noise-free template profile. This template is constructed by fitting von-Mises functions to a high signal-to-noise ratio observation of the pulsar, presenting as an idealized representation of the expected pulse profile (Song et al., 2021). Nevertheless, there exist variations in the data quality obtained from the MeerKAT and Lovell telescopes.

The sensitivity of a telescope is a quantification of its ability to detect electromagnetic radiation emanating from celestial sources in the sky. This attribute is closely tied to the telescope's aperture size and holds significant importance in observational capabilities. The sensitivity of a telescope exhibits a direct proportionality to its collecting area, determined by the diameter of the dish. Consequently, double the aperture size results in a fourfold increase in the collecting area, thereby enhancing sensitivity.

The Lovell telescope is characterized by a singular-dish antenna with a diameter of 76 meters. In contrast, the MeerKAT operates as a radio interferometer, comprising a network of 64 antennas, each with an individual dish diameter of 13.97 meters. Therefore, it is evident that the MeerKAT telescope exhibits a higher sensitivity compared to the Lovell telescope. Moreover, the tied-array beam mitigates interfering signals by inducing dephasing. This heightened sensitivity, coupled with its tied-array beam capabilities, empowers MeerKAT to capture faint astronomical signals and discern more critical details within the observed sources (Bailes et al., 2020).

The pulsar timing initiative at Jodrell Bank commenced in 1975, as documented by Bailes et al. (1993), and has consistently been monitoring around 800 pulsars. The Jodrell Bank Observatory database encompasses a vast dataset of 30,000 Times of Arrivals (ToAs), spanning 17,000 years of pulsar rotational history (Niţ u et al., 2022). On the contrary, the MeerKAT telescope, inaugurated in 2018, is a relatively recent addition and lacks the extended data history present in observations conducted with the Lovell telescope.

Chapter 3

Methodology

3.1 TEMPO2: A Pulsar Timing Software

TEMPO2 is a high-precision pulsar timing tool developed by an international team of researchers (Hobbs et al., 2010). TEMPO2 is designed to produce timing results to better than 1ns precision (Hobbs et al., 2006). It also accounts for clock corrections, different propagation delays, and other phenomena that will be mentioned in this section (Edwards et al., 2006).

To represent the timing in an inertial frame of reference, TEMPO2 converts the ToA at the observatory (t_{obs}) to barycentric arrival times (t_{SSB}). These ToA are compared with the timing model to obtain the timing residuals and perform the weighted least-squares fitting. Another feature of TEMPO2 is that it allows you to compare ToAs obtained at different observatories. However, due to the different systems and receivers at different observatories, there is an offset between the ToAs while being compared. This offset is otherwise known as the "jump" and can be fitted in TEMPO2.

ToAs are measured at different observatories with their local clocks and clock corrections (t_{corr}) that are precise on shorter timescales. As pulsar timing requires very precise measurements, it is not possible to use these clocks over long timescales and while comparing ToAs from different observatories. To avoid this, the ToAs are transformed to a chosen realization of terrestrial time (TT). The atomic timescale (TAI) maintained by the Bureau International des Poids et Mesures (BIPM), is used as a realisation of the theoretical timescale TT. It is done using a database of ASCII files that contain information about the offset between the clocks.

There are different types of propagation delays (Δ_A) caused by the Earth and other objects in space. The tropospheric propagation delay is classified into 2 components based on the dry and wet components present in the region: Hydrostatic and wet delay. `TEMPO2` accounts for the hydrostatic and wet delay, provided that the atmospheric and zenith wet delay data, respectively, are available at the observatory. If not provided, `TEMPO2` considers a standard atmospheric pressure of 1 atm to calculate the hydrostatic delay and negates the effect of the wet delay.

General relativistic effects lead to three delays that are: Einstein Delay ($\Delta_{E\odot}$), Roemer Delay ($\Delta_{R\odot}$), and Shapiro Delay ($\Delta_{S\odot}$).

Einstein delay measures the delay in arrival times, as the clocks at the observatory and the solar system barycentre (SSB) have different clock variations. To resolve this, it is recommended to use barycentric coordinate time (TCB), rather than barycentric dynamical time (TDB) used in `TEMPO1`. By default, `TEMPO2` uses TCB and allows users to convert the timing results obtained in TDB (usually using `TEMPO1`) to TCB using an available TRANSFORM plug-in.

TCB and TDB are both time scales designed to account for relativistic effects, but distinctions exist between them. TCB is designated as the coordinate time at the solar system barycenter, offering a consistent time scale. Conversely, TDB closely resembles TCB but incorporates corrections for gravitational time dilation effects resulting from the motion of Earth and other celestial bodies. In our specific observational context, focusing on distant celestial objects, the gravitational time dilation effects prove negligible. Consequently, we favor TCB over TDB to achieve a more uniform time scale.

Roemer delay refers to the time delay between the ToA of pulses at the observatory and the SSB. This delay is measured by converting the ToAs in 2 steps. To begin with, the time delay between the arrival at the observatory and the Earth's center is measured. Then it is converted to the SSB using the solar system ephemeris provided by NASA Jet Propulsion Laboratories (JPL). For this purpose, `TEMPO2` uses the updated JPL DE405 solar system ephemeris instead of the outdated JPL DE200. In our study, we have used the most recently updated JPL DE440 solar system ephemeris.

As we do high-precision pulsar timing, it is better to use the ephemeris which includes all the objects in the solar system. As the pulses travel through different gravitational fields of heavy objects, there is a delay with the arrival of pulses. This delay is referred to as the Shapiro delay. `TEMPO2` accounts for all objects in the solar system that cause a delay greater than 0.1ns. The objects in the Solar System

that cause the largest delays are the Sun (< 110 μs), Jupiter (< 180 ns), Saturn (< 58 ns), Neptune (< 12 ns) and Uranus (< 10 ns).

There are delays caused due to the frequency at which the observation is taken. TEMPO2 allows fitting these frequency-dependent delays by fitting it to $f^{-\alpha}$, where α is the index for frequency-dependent delays and can be set by the user based on the parameter. For example, dispersion measure delays exhibit an α value of 2, while delays arising from refractive and diffractive effects have an α value of 4 (Foster & Cordes, 1990).

ToA measured with respect to the SSB is given by equation 3.1:

$$t_{SSB} = t_{obs} + t_{corr} + \Delta_A + \Delta_{E\odot} + \Delta_{R\odot} + \Delta_{S\odot} - D/f^2 \tag{3.1}$$

where D/f^2 is the delay due to frequency dispersion in arrival time from the ionised interstellar medium. For a binary system, extra terms that explain the orbital motion are added.

3.1.1 Timing Residuals using TEMPO2

Once the ToAs are converted to barycentric arrival times, the pulse phase of emission with respect to time ($\phi(t)$) is modelled using a Taylor series expansion, given by equation 3.2:

$$\phi(t) = \phi_o + \sum_{n\geq 1} \frac{\nu^{(n-1)}}{n!}(t_p - t_{epoch})^n \tag{3.2}$$

where ν is the rotational frequency, t_p is the pulse emission time and t_{epoch} is a reference epoch. Within our study, the model incorporates two parameters: the rotational frequency ($F0$) and its first derivative, the spin-down rate ($F1$). In instances where a sinusoidal pattern is detected over the course of a year, fitting is also performed for the right ascension (RA) and declination (DEC).

TEMPO2 compares the pulse ToA to an existing timing model to obtain the pre-fit timing residual using equation 3.3:

$$R_i = \frac{\phi_i - N_i}{\nu} \tag{3.3}$$

where ϕ_i is the pulse phase of i'th observation, N_i is the nearest integer to ϕ_i. TEMPO2 improves the timing residuals and the parameter estimation by an iterative post-fit routine using the weighted least-squares algorithm:

$$\chi^2 = \sum_{i=1}^{N} (\frac{R_i}{\sigma_i})^2 \tag{3.4}$$

where N is the number of observations and σ_i is the uncertainty of the i'th observation.

TEMPO2 needs a parameter file and an arrival time file to obtain the timing residuals. Every parameter file (.par) must consist of information about the pulsar's name ($PSRJ$), coordinates on the sky (RA & DEC) in the epoch of J2000, spin-frequency ($F0$), dispersion measure (DM) and the epoch of the measurement ($PEPOCH$). Other than these, extra information about the frequency derivatives and information related to binary pulsars can be added to it. One of the parameter files used in this work is shown below:

```
PSRJ    J1801-2920
RAJ     18:01:46.835
DECJ    -29:20:38.6
F0      0.924292603138   5.000e-12
DM      125.613          1.400e-2
PEPOCH  50549.00000000000000000000
UNITS   TDB
```

The arrival time files consist of information about the arrival time of each pulse and some other relevant information. In general, the arrival time files (.tim) do consist of information about the file name, observing frequency (MHz), Pulse ToA (MJD), the uncertainty (μs), and information about the site of the observatory including the systems used. One of the arrival time files used in this work is shown below:

```
FORMAT 1
file1   1520.000   58440.59762634681914   137.380   jbdfb -be   jbdfb -f   741227124
file2   1520.000   58914.30756731597110   192.679   jbdfb -be   jbdfb -f   759057249
file3   1520.000   59112.78748185284574   247.915   jbdfb -be   jbdfb -f   774907731
```

The processing of certain historical data was performed utilizing `TEMPO1`, given that `TEMPO2` was introduced prior to the construction of MeerKAT. Consequently, the timing models within these datasets are expressed in terms of barycentric dynamical time (TDB). To convert this to barycentric coordinate time (TCB), the built-in `TRANSFORM` plugin can be applied with the following command:

```
tempo2 -gr transform old_filename.par new_filename.par
```

The `new_filename.par` will contain values in terms of TCB and can be used with `TEMPO2`.

`TEMPO2` combines the pre-fit parameter and arrival time file in a graphical interface known as `PLK` with the following command:

```
tempo2 -gr plk -f PulsarName.par PulsarName.tim
```

This interface empowers users to manipulate and process data, facilitating the derivation of post-fit timing residuals. By simply right-clicking, users can eliminate undesired or corrupted data points, particularly those with considerable uncertainties, prior to the fitting process. After ensuring data cleanliness, users can choose specific parameters, such as $F0$ and $F1$ in our study, and execute the program. In instances where timing residuals exhibit an annual periodicity, parameters like RA and DEC are selected for fitting. Subsequently, the graphical interface enables the creation of a new parameter file containing the post-fit residuals.

3.2 Measuring Spin Frequency Derivative ($\dot{\nu}$)

In light of the considerations outlined in section 1.4, we intend to employ the most recent Bayesian Inference package, in conjunction with another independent technique called Fitwaves analysis. Detailed explanations of both methodologies can be found in subsections 3.2.1 and 3.2.2, respectively.

3.2.1 Measuring $\dot{\nu}$ using Bayesian Inference

The posterior distribution of a model is crucial for running a Bayesian inference analysis. It serves as the revised probability distribution of the model parameters, incorporating both the observed data and any prior information available. In this case, $\boldsymbol{\theta}$ denotes the parameters, while $\boldsymbol{D}$ represents the observed data. The posterior distribution ($P(\boldsymbol{\theta}|\boldsymbol{D})$) is obtained using the Bayes' theorem, as shown by equation 3.5:

$$P(\boldsymbol{\theta}|\boldsymbol{D}) = \frac{P(\boldsymbol{D}|\boldsymbol{\theta}) \cdot P(\boldsymbol{\theta})}{P(\boldsymbol{D})} \tag{3.5}$$

To clarify the components of the formula, a detailed explanation of each term is provided. $P(\boldsymbol{\theta})$ represents the initial information, conveying the prior probability of the model parameters prior to data observation. $P(\boldsymbol{D}|\boldsymbol{\theta})$ signifies the likelihood of the observed data, indicating the probability of the observed data given a specific set of model parameters. $P(\boldsymbol{D})$ denotes the marginal likelihood or model evidence, reflecting the probability of the observed data irrespective of the parameter selection. Additionally, it functions as a normalization factor to ensure that the posterior distribution integrates to 1.

Given that the inherent features in the data are distributed across various frequencies i.e., the frequency domain, we employ Fourier-domain Gaussian process modeling in our research. In employing this method, we analyze the timing residuals of the pulsars to obtain the variation in $\dot{\nu}$ using an existing pulsar timing software, `RUN-ENTERPRISE`. Additional details regarding the software can be found at Keith et al. (2022). For this study, we sample the noise parameters using the `EMCEE` ensemble Markov Chain Monte Carlo (MCMC) sampler to generate samples from the posterior distribution (Foreman-Mackey et al., 2013) using 32 independent chains in order to explore the parameter space.

The timing noise is evident as a consistent red noise pattern in the long-term rotational behavior of the pulsar, typically manifesting as a stochastic stationary red noise process (eg. Shannon & Cordes (2010)). The red noise is characterized using a power-law (Niţ u et al., 2022),

$$P(f) = \frac{(A^2)}{12\pi^2} \left(\frac{f}{1\mathrm{yr}^{-1}}\right)^{-\gamma} \tag{3.6}$$

where, A is the amplitude, f is the fluctuation frequency of the noise model, γ is the spectral index and $P(f)$ power spectral density at frequency f.

The spectral index essentially quantifies the rate at which the power in the noise decreases with increasing frequency. It provides insights into the nature of the processes contributing to the observed variability in the pulsar's rotational behavior (Bates et al., 2013). As indicated in Keith & Niţu (2023), when γ exceeds 4, the $\dot{\nu}$ timeseries display residual red noise, leading to the identification of periodicity. Therefore, we impose a minimum value of γ set to 4. The timing noise is then partitioned into bins of log-periods, and `RUN-ENTERPRISE` is executed for each bin, fitting the red noise while

maintaining a minimum value of $\gamma = 4$. Consequently, variations in $\dot{\nu}$ are obtained through this methodology.

For each pulsar, the parameters spin frequency (F0), spin frequency derivative (F1), along with the position (RA and DEC) and clock offsets, representing the "jumps" between different telescopes, were determined through fitting using `TEMPO2`, as outlined in subsection 3.1.1.

3.2.2 Measuring $\dot{\nu}$ using `FITWAVES`

In the fitwaves methodology, we employ harmonically related sinusoids to fit the timing residuals, determining the number of sinusoids based on the structure of the residuals. The estimation of $\dot{\nu}$ is carried out using the harmonic whitening method described in Hobbs et al. (2004), with the distinction that we bootstrap this process using `TEMPO2` to derive the $\dot{\nu}$ values.

Initiating the procedure involves using the timing residuals obtained through `TEMPO2`, as described in subsection 3.1.1. The harmonic whitening package is then executed, specifying the number of sinusoids based on the characteristics of the timing residuals. Initially, this fitting yields whitened residuals and updates the pulsar ephemeris by fitting it to a timing model, minimizing differences between the model and the observed data. Subsequently, the whitening process is reversed, and the residuals are refitted to the timing model, holding the astrometric and dispersion measure constant, to obtain non-whitened residuals.

Assuming all the Times of Arrival (ToAs) have a Gaussian distribution, applying the harmonic whitening package for N iterations results in non-uniformly sampled data points and N smooth curves. Taking the double derivative of these curves provides an estimate of $\dot{\nu}$.

As highlighted in Hobbs et al. (2004), the fitwaves method performs suboptimally when the data are sampled irregularly. Given that the Jodrell Bank Observatory (JBO) data exhibits irregular sampling, we restrict the application of the fitwaves procedure to the MeerKAT dataset in this study.

3.3 Objectives

The objectives of this dissertation are:

1. Obtain the revised ephemerides of the pulsars examined in the research.

2. Measure the variations in spin frequency derivatives through the application of two distinct methodologies: Bayesian Inference and Fitwaves.

3. Evaluate and compare the results derived from diverse datasets to assess the potential benefits of each method, as well as the implications of generating the third dataset as mentioned in section 4.2.

Chapter 4

Results

4.1 Post-fit Timing residuals using TEMPO2

The study commenced with an initial set of 515 pulsars identified through the TPA program. Pulsars with fewer than five observations were subsequently excluded, leading to the selection of 179 pulsars on the basis of this criterion.

Utilizing the methodology outlined in section 3.1.1, post-fit timing residuals for the selected 179 pulsars were derived by fitting for $F0$ and $F1$. In certain cases, RA and DEC were also fitted, particularly when a sinusoidal pattern was detected over the course of a year. The updated ephemerides for these pulsars are presented in Table 4.1.

4.2 Estimation of $\dot{\nu}$ variations

To estimate the spin frequency derivatives, we use three different datasets:

1. Timing data from the Jodrell Bank Observatory (JBO)
2. Timing data from the MeerKAT telescope
3. A combined dataset of both Jodrell Bank and MeerKAT telescopes

Due to the considerations outlined in section 2.4, specifically the enhanced sensitivity and resolution provided by MeerKAT, along with the extensive data history from the Jodrell Bank timing program, we opted to compile a third dataset that incorporates both timing data for subsequent analysis. This third dataset was not directly accessible. Consequently, to obtain the integrated dataset from the

TABLE 4.1: Updated ephemerides of 179 pulsars. The pulsar's name is followed by the right ascension and declination in J2000 coordinates, the pulsar's rotational parameters, the reference epoch in Modified Julian Date (MJD), and the final RMS value for the timing residuals.

PSR J	RA (J2000) (h:m:s)	Dec. (J2000) (° : ′ : ″)	ν (s^{-1})	$\dot{\nu}$ ($10^{-15}\ s^{-2}$)	$\ddot{\nu}$ ($10^{-24}\ s^{-3}$)	t_{epoch} (MJD)
J1801-0357	18:01:23.155(4)	-03:58:28.61(3)	1.0851	-3.931(6)	-0.032(7)	59053
J1801-2920	18:01:46.835	-29:20:38.6	0.9242	-2.219(2)	-0.0185 (6)	59092
J1802-1745	18:02:14.85(3)	-17:45:17(7)	1.9429	-2.137(2)		58766
J1805-0619	18:05:31.436(9)	-06:19:45.4(4)	2.1994	-4.704(3)		59097
J1806-1154	18:06:06.7801(9)	-11:54:29.83(9)	1.9134	-5.1501(5)	0.0084(5)	59020
J1807-0847	18:07:38.01743(4)	-08:47:43.24(2)	6.1077	-1.0749(6)	-0.0047(2)	59038
J1807-2715	18:07:08.495	-27:15:03	1.208	-17.8043(3)	-0.082(3)	59092
J1808-0813	18:08:09.406(2)	-08:13:01.49(8)	1.1414	-1.609(1)	0.002(2)	59020
J1808-1020	18:08:45.634(6)	-10:20:48.3(4)	1.6750	-2.135(7)		58766
J1808-1517	18:08:39.09(2)	-15:17:40(1)	1.8363	-8.9902(9)		58949
J1808-3249	18:08:04.48(2)	-32:49:34(1)	2.7403	-52.874(3)		59130
J1809-1429	18:09:45.510(8)	-14:29:25(1)	1.1169	-6.499(5)		58976
J1811-0154	18:11:19.88(3)	-01:54:30.9(7)	1.0811	-1.9252(2)		59097
J1811-4930	18:11:27.19(1)	-49:30:20.8(2)	0.6979	-1.1001(7)		59101
J1812-1733	18:12:15.85925(7)	-17:33:370.871(2)	1.8575	-3.3925(7)	-0.014(5)	58912
J1813-2113	18:13:39.87(3)	-21:13:00.4(3)	2.3448	-11.424(2)		58976
J1817-3618	18:17:05.863(2)	-36:18:05.427(5)	2.5838	-13.6206(3)		59031
J1817-3837	18:17:00.2864(9)	-38:38:00.357(9)	2.6008	-3.9073(8)		59031
J1819+1305	18:19:56.226(3)	+13:05:15.25(1)	0.943	-0.4127(7)		59024
J1819-0925	18:19:50.542(9)	-09:25:49.9(3)	1.1736	-4.283(5)		59097
J1819-1114	18:19:28.78(1)	-11:14:43(1)	3.3994	-6.5131(7)		59046
J1820-0427	18:20:52.588	-04:27:37.095	1.672	-17.707(3)	0.0357(9)	59108
J1820-1818	18:20:39.074(1)	-18:18:02.757(7)	3.2267	-0.9744(1)	0.0056(7)	59020
J1822-4209	18:22:11.356(3)	-42:09:10.98(7)	2.1905	-2.188(2)		53121
J1823+0550	18:23:30.9654(2)	+05:50:24.22(4)	1.3281	-0.4016(3)	-0.00005(7)	59097
J1823-0154	18:23:52.146	-01:54:04.6	1.3161	-1.9583(7)	-0.0106(2)	59020
J1823-3106	18:23:46.822	-31:06:49.089	3.5204	-36.3165(1)	-0.201(9)	59031
J1824-0127	18:24:53.43(4)	-01:27:51.4(8)	0.4008	-0.6281(3)		59101
J1824-1159	18:24:56.151(2)	11:59:53.4(3)	2.7586	-42.0443(3)		58808
J1824-1945	18:24:00.477	-19:45:51.449	5.2815	-145.9466(4)	0.052(2)	59031
J1825+0004	18:25:15.37(1)	+00:04:20.14(4)	1.2837	-1.4516(4)	0.00168	52500
J1825-1446	18:25:02.96186(2)	-14:46:53.4912(2)	3.5815	-290.724(4)	0.224(9)	59108
J1826-1131	18:26:05.472	-11:31:43.6	0.4777	-1.1192(4)	0.0069(4)	59020
J1827-0934	18:27:45.884(6)	-09:34:16.4(3)	1.951	-27.482(3)		58812
J1828-0611	18:28:20.715(6)	-06:11:51.5(4)	3.7117	-20.090 (5)		59020
J1829-0734	18:29:05.3762(8)	-07:34:19.72(2)	3.1406	-47.33(1)		58949
J1829-1751	18:29:43.175	-17:51:07.643	3.2558	-58.779(1)	0.033(9)	58993
J1830-1059	18:30:47.566	-10:59:27.9	2.4685	-364.858(8)	0.872(9)	59115
J1831-0823	18:31:36.334(8)	-08:23:23.9(5)	1.6336	-0.8337(3)		59020
J1832-0644	18:32:42.624(3)	-06:44:00.967(2)	1.3435	-66.829(2)		58976

PSR J	RA (J2000) (h:m:s)	Dec. (J2000) (° : ′ : ″)	ν (s^{-1})	$\dot{\nu}$ (10^{-15} s^{-2})	$\ddot{\nu}$ (10^{-24} s^{-3})	t_{epoch} (MJD)
J1832-0827	18:32:37.0129	-08:27:03.114	1.5447	-152.518 (1)	0.019(1)	59031
J1833-0338	18:33:41.886	-03:39:04.407	1.4561	-88.209 (9)	0.143(1)	59142
J1833-0827	18:33:40.3	-08:27:31.25	11.7245	-1262.1799(1)	-1.301(2)	59031
J1834-0426	18:34:25.602	-04:26:15.84	3.4469	-0.850(2)	0.016(3)	49714
J1834-0742	18:34:31.32(3)	-07:42:20.6(4)	1.2684	-52.214(7)		59106
J1834-1202	18:34:23.0802(2)	-12:02:25.09(9)	1.6386	-0.0193(4)		58976
J1835-1020	18:35:57.6017(4)	-10:20:03.94(9)	3.3063	-64.728(8)		59097
J1835-1106	18:35:18.038(2)	-11:06:22.6(2)	6.0306	-746.2(1)		49445
J1836-0436	18:36:51.79	-04:36:37.68	2.8229	-13.2333(5)	-0.087(6)	59020
J1837+1221	18:37:07.12(4)	+12:21:54.0(6)	0.5092	-1.6023(6)		59110
J1837-0045	18:37:32.154	-00:45:10.6	1.6206	-4.4308(3)	-0.0038(6)	59187
J1837-0559	18:37:23.663(4)	-05:59:28.3(9)	4.9735	-81.914(6)		59110
J1837-0653	18:37:14.65	-06:53:02.1	0.5247	-0.2165(4)	0.00046(9)	59020
J1837-1837	18:37:54.25(1)	-18:37:08(2)	1.6171	-14.4338(7)		58949
J1839-1238	18:39:43.708(9)	-12:38:40.7(8)	0.5231	-1.3503(4)		59110
J1840-0809	18:40:33.364(6)	-08:09:03.3(4)	1.0463	-2.57306(9)		59097
J1840-0815	18:40:13.775(3)	-08:15:10.6(7)	0.912	-2.023(1)		59097
J1841+0912	18:41:55.9515(9)	+09:12:07.858(5)	2.6224	-7.5332(4)	0.0635(1)	59101
J1841-0157	18:41:56.21(2)	-01:57:54.6(8)	1.5075	-41.058(4)		59097
J1842+1332	18:42:29.96(6)	+13:32:01.5(9)	2.1204	-0.971(6)		59101
J1842-0359	18:42:26.477	-03:59:59.8	0.5434	-0.1493(5)	0.00098(3)	59097
J1842-0905	18:42:22.138(7)	-09:05:24.6(8)	2.9015	-88.068(2)		59038
J1843-0000	18:43:27.962(9)	-00:00:40.9(6)	1.1359	-9.993(2)		59097
J1843-0211	18:43:30.304(2)	-02:11:02.93(4)	0.4932	-3.5088(4)		59020
J1843-0459	18:43:27.643(8)	-04:59:30.4(3)	1.3245	-1.5006(6)		59020
J1844+1454	18:44:54.878(1)	+14:54:15.31(3)	2.6633	-13.282(9)	0.06(7)	59101
J1844-0030	18:44:41.099(9)	-00:30:25.8(3)	1.5598	-14.758(9)		59113
J1844-0433	18:44:33.452	-04:33:12.4	1.009	-3.9854(3)	-0.0015(4)	59097
J1845+0623	18:45:08.59(3)	+06:23:57.6(9)	0.7034	-0.27083(7)		59113
J1845-0434	18:45:34.709	-04:34:29.8	2.0544	-47.820(4)	0.010(8)	59108
J1845-0545	18:45:38.49(4)	-05:45:18.2(1)	0.9154	-11.338(8)		59113
J1845-0635	18:45:07.406(9)	-06:35:23.4(8)	2.9366	-38.746(1)		58949
J1845-0743	18:45:57.18(1)	-07:43:38.4(6)	9.5515	-33.472(2)		59031
J1845-1114	18:45:45.778(6)	-11:14:11.0(5)	4.8491	-47.1701(9)		59189
J1846+0051	18:46:43.82(2)	+00:51:39.0(7)	2.3021	-59.473(1)		59113
J1847-0402	18:47:22.8418(16)	-04:02:14.14(6)	1.6727	-144.62(4)	0.0797(5)	59034
J1847-0438	18:47:37.925(3)	-04:38:15.3(9)	1.0438	-11.9124(6)		59113
J1847-0605	18:47:21.071(1)	-06:05:14.1(9)	1.285	-7.6535(6)		59097
J1848+0604	18:48:54.622(7)	+06:04:46.8(3)	0.4507	-0.7721(3)		59113
J1848-0023	18:48:37.89(9)	-00:23:17.0(4)	1.86	-5.562(4)		59053
J1848-0123	18:48:23.594(1)	01:23:58.69(5)	1.5164	-11.956(1)	-0.018(7)	59034
J1849-0317	18:49:57.85(3)	-03:17:31.0(3)	1.496	-49.428(4)		58977
J1849-0614	18:49:45.157(9)	-06:14:31.5(8)	1.0488	-59.595(9)		59189
J1850+0026	18:50:45.14(1)	+00:26:25.6 (9)	0.9243	-0.3046(8)		59020
J1851+0418	18:51:03.298	+04:18:12.0	3.5124	-13.4893(6)	0.224(5)	59044

PSR J	RA (J2000) (h:m:s)	Dec. (J2000) (° : ′ : ″)	ν (s^{-1})	$\dot{\nu}$ ($10^{-15}\ s^{-2}$)	$\ddot{\nu}$ ($10^{-24}\ s^{-3}$)	t_{epoch} (MJD)
J1851+1259	18:51:13.215	+12:59:35.29	0.8296	-7.8203(1)	0.147(1)	59101
J1851-0029	18:51:55.09(1)	-00:29:58.1(5)	1.9278	-17.4697(9)		59113
J1851-0053	18:51:03.270(2)	-00:53:07.3(1)	0.7096	-0.4295(7)		59020
J1853-0004	18:53:23.018(6)	-00:04:32.3(4)	9.8581	-541.9012(9)		59115
J1855+0307	18:55:26.63(3)	+03:07:20.2(9)	1.1829	-25.307(2)		59024
J1855-0941	18:55:15.68(3)	-09:41:02.0(1)	2.8951	-1.9753(9)		59078
J1856-0526	18:56:21.977(5)	-05:26:56.8(8)	2.6991	-12.103(2)		59026
J1857+0057	18:57:00.8	+00:57:16.8	2.8016	-0.4384(5)	-0.004(4)	59024
J1857+0212	18:57:43.642	+02:12:41.11	2.4046	-2.3272(3)	0.278(5)	59024
J1900+0634	19:00:28.03(2)	+06:34:20.9(6)	2.5649	-33.772(4)		59118
J1900-0051	19:00:46.644(7)	-00:51:08.4(5)	2.596	-0.9539(7)		59118
J1900-2600	19:00:47.540(4)	-26:00:45.1(5)	1.6334	-0.55051(9)	-0.00276(4)	59038
J1901+0124	19:01:52.545(4)	+01:24:49.3(8)	3.1365	-31.973(7)		59118
J1901+0156	19:01:34.2983(6)	+01:56:38.509(4)	3.4695	-28.462(2)	-0.012463	59118
J1901+0331	19:01:31.774(2)	+03:31:05.39(7)	1.5256	-17.4559(6)	0.324(6)	59029
J1901+0716	19:01:38.936	+07:16:34.8	1.5527	-5.517(3)	0.356(4)	59026
J1901-0906	19:01:53.015	-09:06:10.8	0.5611	-0.5165(8)	0.0013(5)	59025
J1902+0615	19:02:50.277(3)	+06:16:33.41(7)	1.4847	-16.998(2)		59101
J1903+0135	19:03:29.985(1)	+01:35:38.20(4)	1.3711	-7.5754(6)		59101
J1903+0601	19:03:20.874(6)	+06:01:34.0(6)	2.6728	-137.433(5)		59118
J1904+0004	19:04:12.7247(5)	+00:04:05.20(4)	7.1671	-6.060(8)		59029
J1904+0738	19:04:07.533(1)	+07:38:51.69(4)	4.7856	-9.3978(4)		59118
J1904+0800	19:04:03.50(2)	+08:00:52.6(9)	3.7971	-249.274(8)		59118
J1904+1011	19:04:02.49(2)	+10:11:34.6(5)	0.5386	-0.0787(8)		59107
J1904-1224	19:04:33.281	-12:24:01.3	1.3318	-1.3306(1)	-0.003(2)	59118
J1905+0600	19:05:04.35(5)	+06:00:59.9(4)	2.2664	-5.675(6)		59120
J1905+0616	19:05:06.849(5)	+06:16:16.7(1)	1.0103	-137.936(6)		59120
J1905-0056	19:05:27.7354	-00:56:40.96	1.5547	-7.3962(5)	-0.0196(8)	59101
J1906+0641	19:06:35.244	+06:41:02.9	3.7414	-29.8929(4)	-0.0068(8)	59029
J1906+0912	19:06:28.46(3)	+09:12:56.6(5)	1.2897	-0.2166(6)		59126
J1907+0740	19:07:44.118(3)	+07:40:22.6(9)	1.74	-2.025(3)		59126
J1908+0909	19:08:07.437(3)	+09:09:12.4(5)	2.971	-307.54(2)	1.2(9)	59120
J1908+0916	19:08:58.76(6)	+09:16:14.0(1)	1.2044	-0.0783(6)		59120
J1909+0007	19:09:35.266	+00:07:56.862	0.9833	-5.3454(5)	0.017(3)	59101
J1909+0254	19:09:38.310	+02:54:50.67	1.0102(1)	-5.6110(3)	0.0741	59115
J1910+0225	19:10:10.359(7)	+02:25:23.6(5)	2.9598	-2.2764(1)		59058
J1910+0358	19:10:09.06	+03:58:28.0	0.4291	-0.81305(8)	0.014(3)	59048
J1910+0714	19:10:18.597(6)	+07:14:11.8(5)	0.3686	-0.832(1)		59133
J1910+0728	19:10:22.079(6)	+07:28:37.09(5)	3.0729	-78.455(6)		59101
J1910+1231	19:10:13.53	+12:31:40.2	0.6936	-3.966(1)	0.0014(5)	59128
J1910-0309	19:10:29.693(5)	-03:09:53.8(3)	1.9817	-8.592(2)	-0.13(8)	59128
J1913+1145	19:13:43.88(6)	+11:45:33.1(1)	3.2672	-53.521(1)		59128
J1913+1400	19:13:24.357	+14:00:52.72	1.9176	-2.9619(2)	-0.0178(1)	59029
J1913-0440	19:13:54.193(2)	-04:40:48.7605(2)	1.2107	-5.9637(5)	0.0161(5)	59110
J1914+0631	19:14:17.24(4)	+06:31:56.3(1)	1.4413	-0.108(2)		59107

PSR J	RA (J2000) (h:m:s)	Dec. (J2000) (° : ′ : ″)	ν (s^{-1})	$\dot{\nu}$ (10^{-15} s^{-2})	$\ddot{\nu}$ (10^{-24} s^{-3})	t_{epoch} (MJD)
J1914+1122	19:14:10.12(1)	+11:22:03.7(2)	1.6638	-1.8(8)		59128
J1915+0227	19:15:02.122(5)	+02:27:47.77(6)	3.1515	-2.9563(2)		59128
J1915+0738	19:15:24.80(2)	+07:38:31.4(8)	0.6482	-1.3846(1)		59128
J1915+0838	19:15:13.87(3)	+08:38:59.7(3)	2.9173	-13.387(6)		591281
J1916+0844	19:16:19.081(9)	+08:44:07.0(4)	2.2727	-14.955 (3)		59129
J1916+0951	19:16:32.339(1)	+09:51:25.851(6)	3.7001	-34.518(6)	-0.0314(9)	59101
J1916+1030	19:16:11.72(1)	+10:30:53.4(6)	1.59	-0.0831(6)		59129
J1917+0834	19:17:48.853(6)	+08:34:54.63(4)	0.4695	-3.8622(9)		59129
J1919+0021	19:19:50.659(5)	+00:21:39.7(2)	0.7859	-4.7418(7)	0.0166(9)	59101
J1919+0134	19:19:43.62(3)	+01:34:56.5(7)	0.6234	-0.2255(2)		59029
J1921+1419	19:21:24.159	+14:19:17.1	1.6176	-14.6337(4)	0.037(3)	59115
J1921+1948	19:21:03.799	+19:48:44.7	1.2179	-1.3272(9)	0.0017(6)	59101
J1922+1733	19:22:53.2046(2)	+17:33:23.59(2)	4.2341	-239.9231(9)		59101
J1923+1706	19:23:07.85(1)	+17:06:09.4(2)	1.8274	-0.1339(6)		59133
J1926+1434	19:26:57.22	+14:34:55.3	0.7547	-0.1218(4)	0.0005(3)	59107
J1926+1648	19:26:45.323(3)	+16:48:32.123(5)	1.7246	-53.5812(9)	0.041(6)	59101
J1927+1852	19:27:10.422(8)	+18:52:08.5(2)	2.0713	-0.483(4)		59107
J1927+1856	19:27:24.97(1)	+18:56:36.8(2)	3.3521	-25.258(7)		59107
J1931+1536	19:31:55.71(1)	+15:36:57.5(3)	3.181	-50.702(5)		59107
J1932+1059	19:32:14.0819(3)	+10:59:33.309(5)	4.4146	22.5405(6)	0.015(3)	59101
J1932-3655	19:32:06.150(8)	-36:55:02.1(4)	1.75	-0.8773(3)		59092
J1933+1304	19:33:22.529(4)	+13:04:49.97(8)	1.0772	-0.3667(6)		59118
J1935+1616	19:35:47.8273(1)	+16:16:39.688(2)	2.7874	-46.6461(6)	0.0144(1)	59029
J1941-2602	19:41:00.4288(8)	-26:02:05.99(2)	2.4822	-5.8918(1)	-0.0078(2)	59038
J1943+0609	19:43:29.132(5)	+06:09:57.6(1)	2.241	-2.3487(4)		59101
J1943-1237	19:43:25.481	-12:37:42.4	1.0283	-1.762(3)	-0.0002(1)	59043
J1945-0040	19:45:28.39	-00:40:58.1	0.9563	-0.4884(4)	0.00005(4)	59101
J1946+1805	19:46:53.045(6)	+18:05:40.98(1)	2.2695	-0.135(7)	0.00002(3)	59101
J1946-2913	19:46:51.775(8)	-29:13:48.0(5)	1.0422	-1.615(2)	-0.00125(8)	59094
J1949-2524	19:49:25.502(5)	-25:24:00.354(9)	1.0442	-3.5673(2)	0.0002(2)	59026
J1956+0838	19:56:52.26(2)	+08:38:16.8(4)	3.2904	-2.4503(5)		59029
J2005-0020	20:05:43.74	-00:20:21.9	0.4386	-4.9457(9)	0.0007(5)	59043
J2006-0807	20:06:16.367	-08:07:01.9	1.7215	-0.1296(3)	-0.0048(5)	59110
J2038-3816	20:38:54.19(3)	-38:16:11.9(1)	0.6339	-1.6618(3)		59054
J2046+1540	20:46:39.323(5)	+15:40:33.69(1)	0.8785	-0.1410(6)	-0.00001(1)	59029
J2046-0421	20:46:00.173(5)	-04:21:26.1(2)	0.6464	-0.6153(3)	0.00016(9)	59029
J2048-1616	20:48:35.74837(4)	-16:16:44.6165(5)	0.5097	-2.8494(1)	-0.00091(8)	59107
J2053-7200	20:53:47.304(4)	-72:00:42.461(4)	2.9296	-1.6964(2)		59019
J2108-3429	21:08:30.49(2)	-34:29:37.9(2)	0.7026	-1.7319(4)		59034
J2116+1414	21:16:13.767(3)	+14:14:20.72(7)	2.2719	-1.5017(5)	-0.0085(5)	59029
J2124+1407	21:24:46.574	+14:07:19.3	1.4408	-1.5987(5)	0.0041(8)	59034
J2127-6648	21:27:31.508(6)	-66:48:28.437(6)	3.0696	-2.124(3)		59034
J2155-3118	21:55:13.61	-31:18:54.7	0.9708	-1.1702(7)	0.0023(4)	59114
J2215+1538	22:15:39.6784(4)	+15:38:34.14(2)	2.6723	-16.904(4)		59034
J2248-0101	22:48:26.904	-01:01:48.1	2.0954	-2.891(4)	0.035(4)	59034

PSR J	RA (J2000) (h:m:s)	Dec. (J2000) (° : ′ : ″)	ν (s^{-1})	$\dot{\nu}$ ($10^{-15}\ s^{-2}$)	$\ddot{\nu}$ ($10^{-24}\ s^{-3}$)	t_{epoch} (MJD)
J2253+1516	22:53:14.533(4)	+15:16:37.83(8)	1.2622	-0.0953(2)		59034
J2324-6054	23:24:27.252(7)	-60:54:06.513(9)	0.4259	-0.4675(2)		59019
J2330-2005	23:30:27.0178(7)	-20:05:29.50(7)	0.6084	-1.7155(9)	0.00003(3)	59029
J2346-0609	23:46:50.454	-06:09:59.5	0.8464	-0.9713(6)	-0.0011(2)	59029

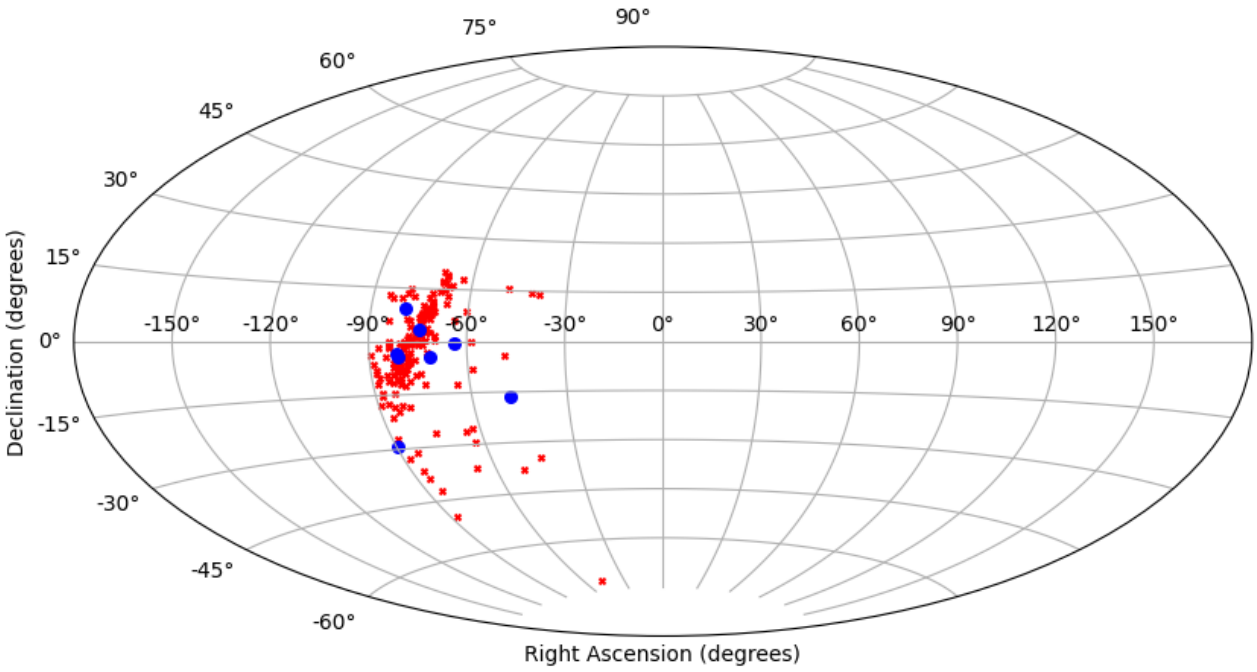

FIGURE 4.1: Aitoff Projection Map of the original pulsar sample provided (depicted with red 'X') and the selected pulsars for analysis (shown with blue 'O')

Jodrell Bank and MeerKAT telescopes, we compiled the timing data from both observatories into a unified `.tim` file.

Given that this research serves as an initial exploratory investigation, the selection of pulsars was guided by the following criteria:

1. Pulsars displaying diverse characteristics in the timing residuals.
2. Consideration of the data span, with a requirement for availability extending beyond 600 days.
3. Pulsars located at distinct locations in the sky, specifically within the TPA dataset I received, which includes pulsars with right ascension (RA) values between 18h and 20h. However, it's important to note that the entire sample only represents a portion of the galactic plane. In Figure 4.1, the Aitoff projection map displays both the original pulsar sample provided (depicted with red 'X') and the selected pulsars for analysis (shown with blue 'O').

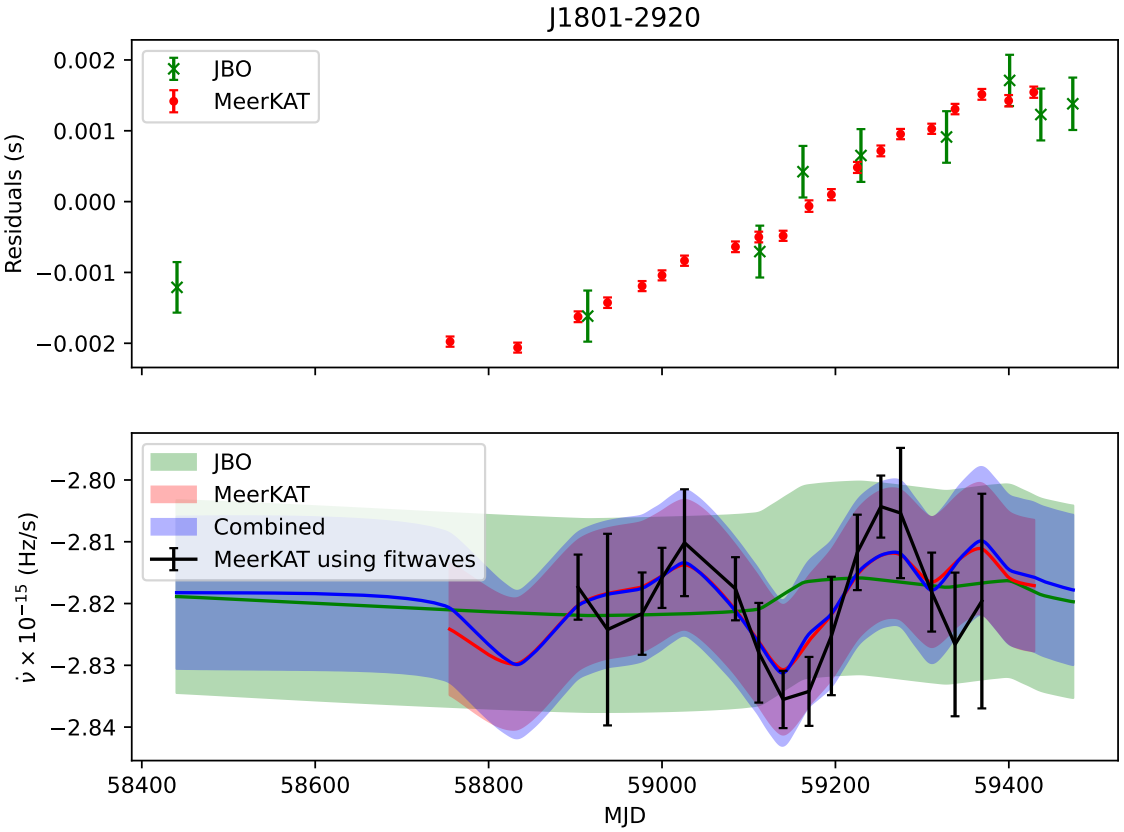

FIGURE 4.2: Timing residuals and $\dot{\nu}$ variations in PSR J1801-2920 using Bayesian and Fitwaves analysis

We have assessed the $\dot{\nu}$ variations for a selection of eight pulsars, based on the criteria mentioned above, employing both Bayesian inference and the fitwaves method, as described in subsections 3.2.1 and 3.2.2, respectively. The outcomes are detailed below. Notably, the fitwaves method was exclusively employed for the MeerKAT dataset, as the remaining datasets exhibit irregular sampling.

4.2.1 Pulsars with $\dot{\nu}$ variations

The timing residuals and $\dot{\nu}$ variations of PSR J1801-2920 are illustrated in Figure 4.2. The oscillation of $\dot{\nu}$ spans a range around a mean value of -2.82×10^{-15} Hz/s. The dip in $\dot{\nu}$ observed around MJD 59150 is visible solely in the MeerKAT data. Due to the limited number of observations from the Jodrell Bank Observatory (JBO) data, the recovery of this feature becomes impossible. Consequently, the combination of JBO and MeerKAT data does not reveal any noticeable variations. Notably, the data from the fitwaves methodology and Bayesian analysis of MeerKAT data exhibit consistency, indicative of a high cadence in observations.

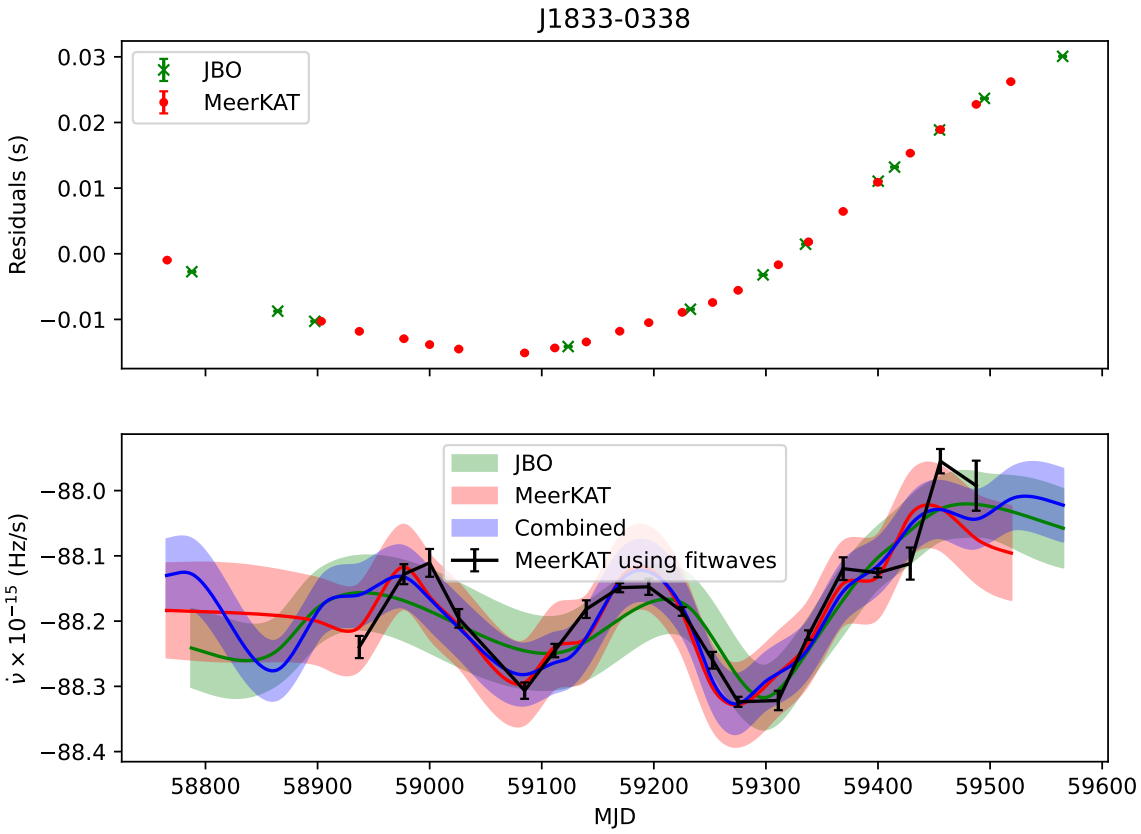

FIGURE 4.3: Timing residuals and $\dot{\nu}$ variations in PSR J1833-0338 using Bayesian and Fitwaves analysis

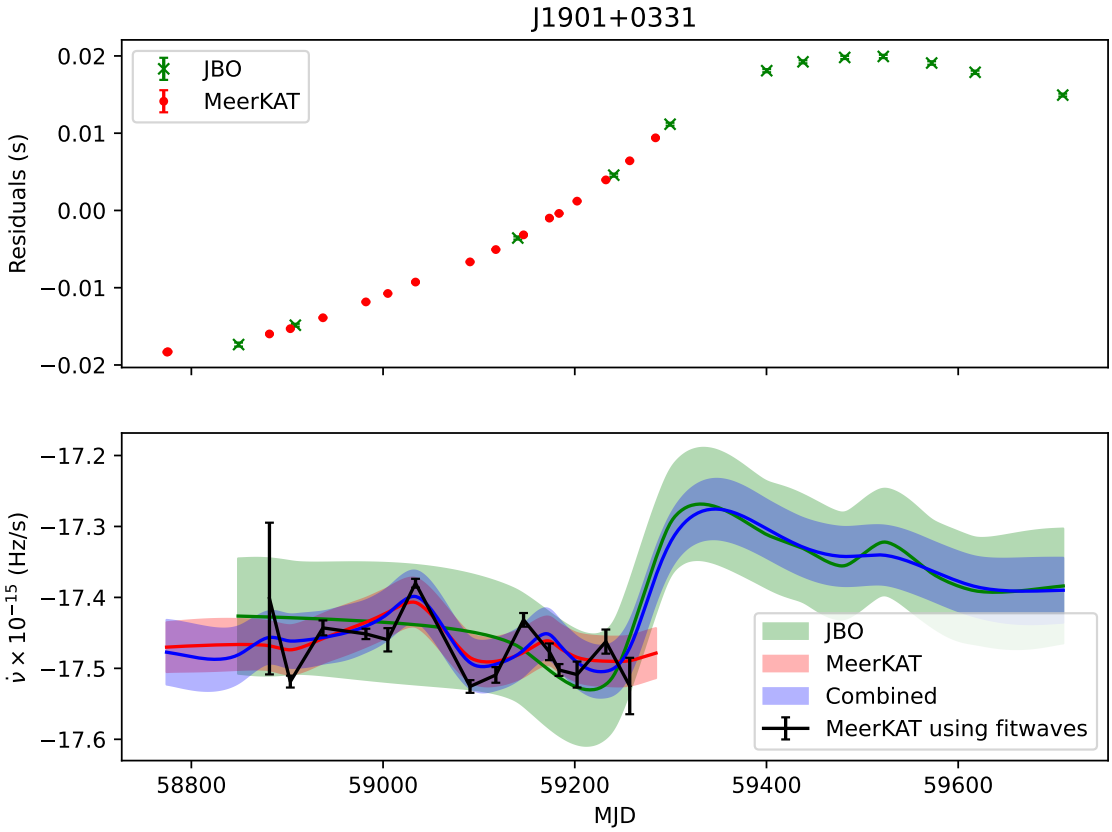

FIGURE 4.4: Timing residuals and $\dot{\nu}$ variations in PSR J1901+0331 using Bayesian and Fitwaves analysis

The timing residuals and $\dot{\nu}$ variations of PSR J1833-0338 are depicted in Figure 4.3. The $\dot{\nu}$ exhibits oscillations around a mean value of -88.2×10^{-15} Hz/s, with discernible variations approximately every 200 days, as indicated by the peaks. In contrast to the previous case, where combining Jodrell Bank Observatory (JBO) and MeerKAT data did not contribute significantly to constraining $\dot{\nu}$, for PSR J1833-0338, the fitwaves method shows reduced uncertainty. The combination of both JBO and MeerKAT data has proven beneficial in refining the measurement of $\dot{\nu}$. Additionally, the consistency between data from the fitwaves method and Bayesian analysis is evident across all datasets.

The timing residuals and $\dot{\nu}$ variations of PSR J1901+0331 are shown in Figure 4.4. Since there are no observations from MeerKAT beyond MJD 59250, the combination of Jodrell Bank Observatory (JBO) and MeerKAT data has proven valuable in identifying a decrease in the spin-down rate. Moreover, the data from the fitwaves method exhibits consistency with the Bayesian analysis between MJD 58850 and 59250. The reduced uncertainties in timing residuals during this period have contributed to refining the measurement of $\dot{\nu}$.

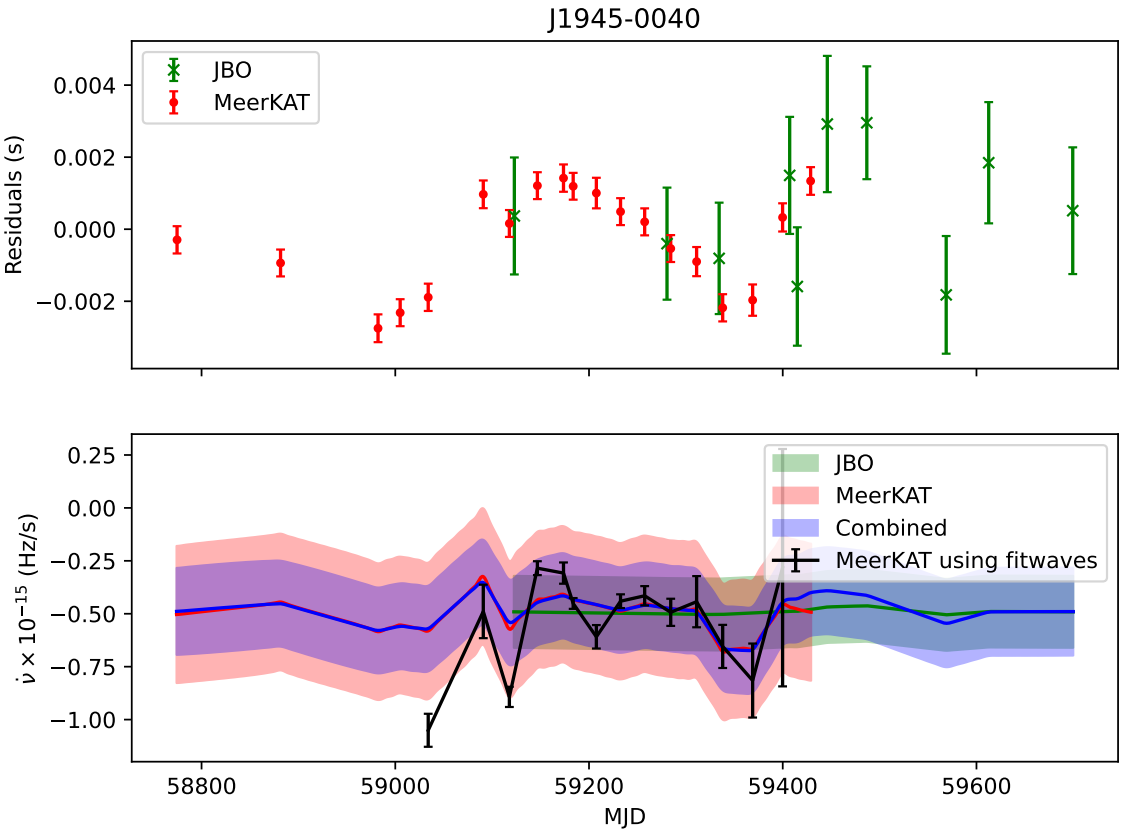

FIGURE 4.5: Timing residuals and $\dot{\nu}$ variations in PSR J1945-0040 using Bayesian and Fitwaves analysis

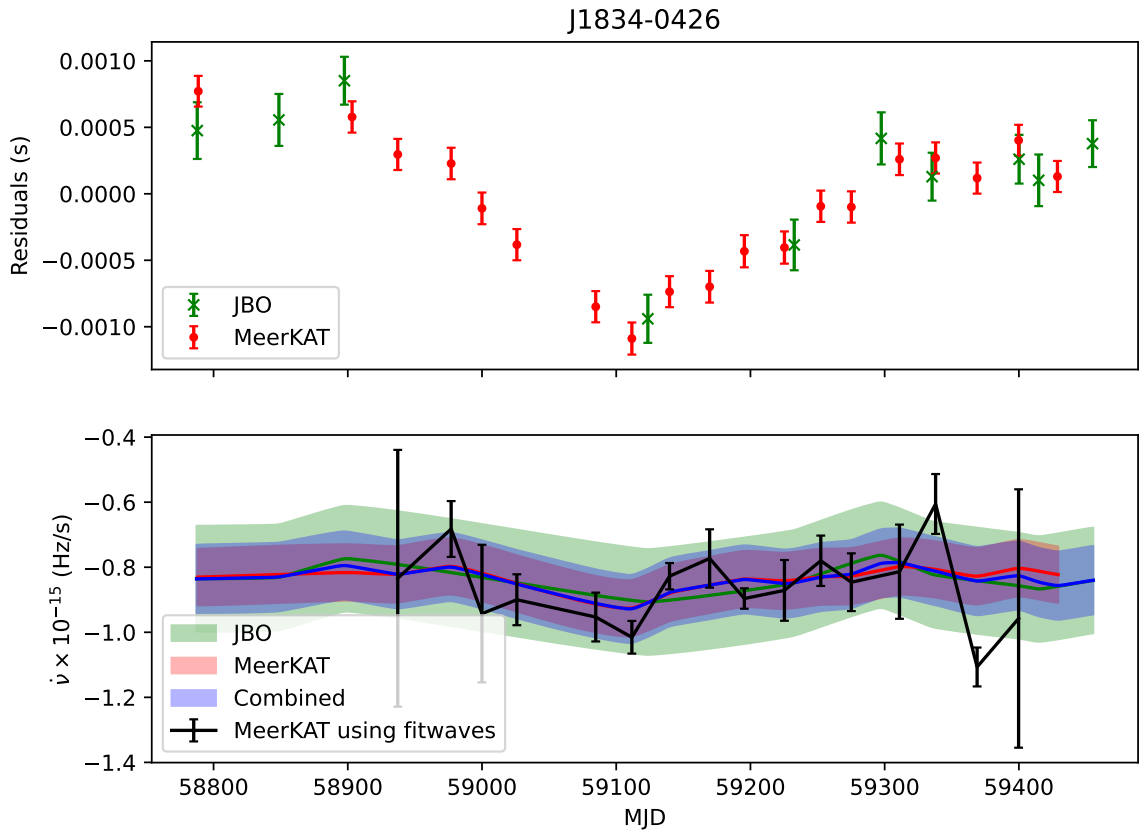

FIGURE 4.6: Timing residuals and $\dot{\nu}$ variations in PSR J1834-0426 using Bayesian and Fitwaves analysis

The timing residuals and $\dot{\nu}$ variations of PSR J1945-0040 are illustrated in Figure 4.5. Featuring a mean $\dot{\nu}$ of -0.5×10^{-15} Hz/s, a minor peak emerges around MJD 59100 with no prominent variations in $\dot{\nu}$. Nevertheless, the variations in $\dot{\nu}$ from both the fitwaves method and Bayesian analysis exhibit consistency across all datasets.

4.2.2 Pulsars with no $\dot{\nu}$ variations

The timing residuals and $\dot{\nu}$ variations of PSR J1834-0426 are displayed in Figure 4.6. This pulsar has a pulse period of 127.50533 ms. With a $\dot{\nu}$ of approximately -0.8×10^{-15} Hz/s, it seems unlikely that significant $\dot{\nu}$ variations exist in this pulsar. In this particular instance, the Jodrell Bank Observatory (JBO) data and the combined dataset provide limited assistance in measuring $\dot{\nu}$ variations. Despite the consistency between the fitwaves and Bayesian techniques, the uncertainty in measuring the variation remains high using the fitwaves methodology.

The timing residuals and $\dot{\nu}$ variations of PSR J1841+0912 are presented in Figure 4.7. With a $\dot{\nu}$ of

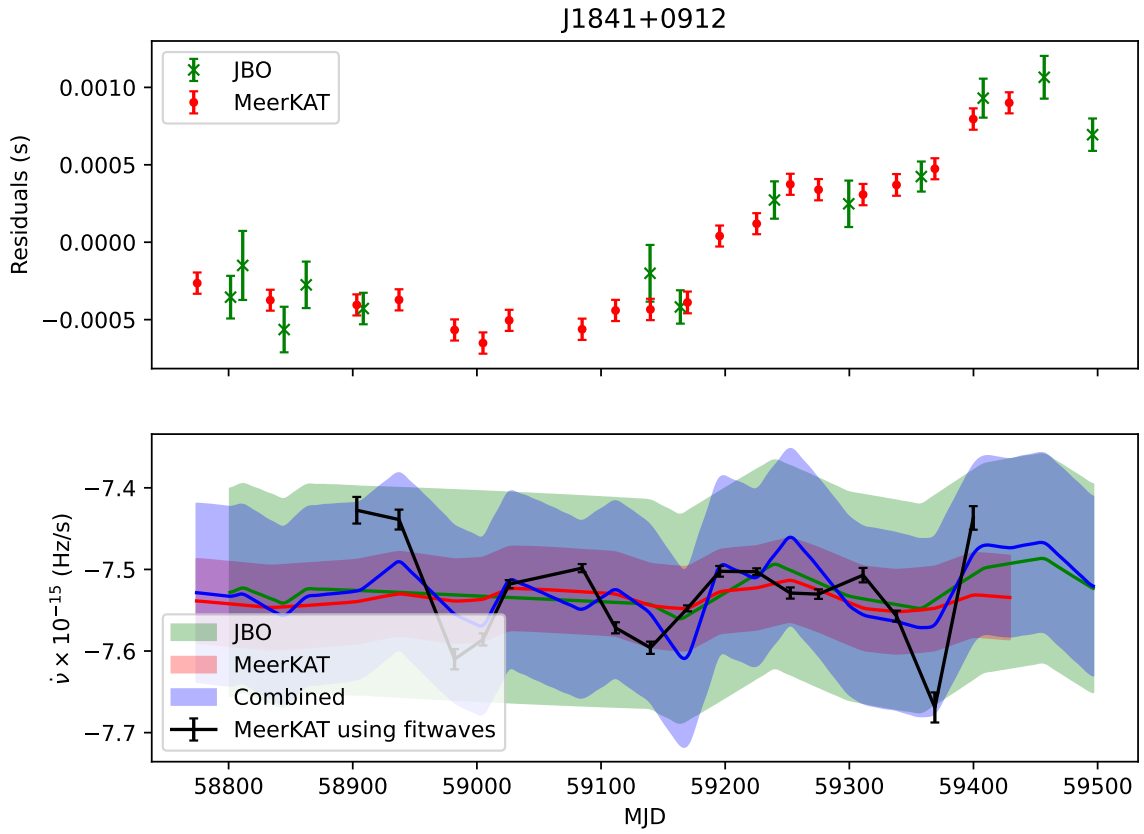

FIGURE 4.7: Timing residuals and $\dot{\nu}$ variations in PSR J1841+0912 using Bayesian and Fitwaves analysis

approximately -7.5×10^{-15} Hz/s, there are no discernible $\dot{\nu}$ variations in this pulsar. In this scenario, it is apparent that the Jodrell Bank Observatory (JBO) data is not contributory, rendering the combination of both JBO and MeerKAT data unhelpful in measuring the $\dot{\nu}$ variations. Nevertheless, the data obtained through the fitwaves methodology and Bayesian analysis of MeerKAT data exhibit consistency. Therefore, it is more effective to utilize only the MeerKAT data for measuring the $\dot{\nu}$ variations.

4.2.3 Special Cases

The timing residuals and $\dot{\nu}$ variations of PSR J1913-0440 and PSR J2048-1616 are presented in Figures 4.8 and 4.9, respectively. PSR J1913-0440 has been consistently observed by the JBO more than MeerKAT. Consequently, utilizing the JBO data and combining it with the MeerKAT data has proven effective in constraining the $\dot{\nu}$ variations. On the other hand, for PSR J2048-1616, the JBO data alone is not informative, and combining it with MeerKAT data yields no significant improvement. Additionally, the timing residuals in this case exhibit near-white characteristics, posing challenges for fitwaves analysis. Notably, in both cases, the fitwaves data shows inconsistency with the Bayesian analysis.

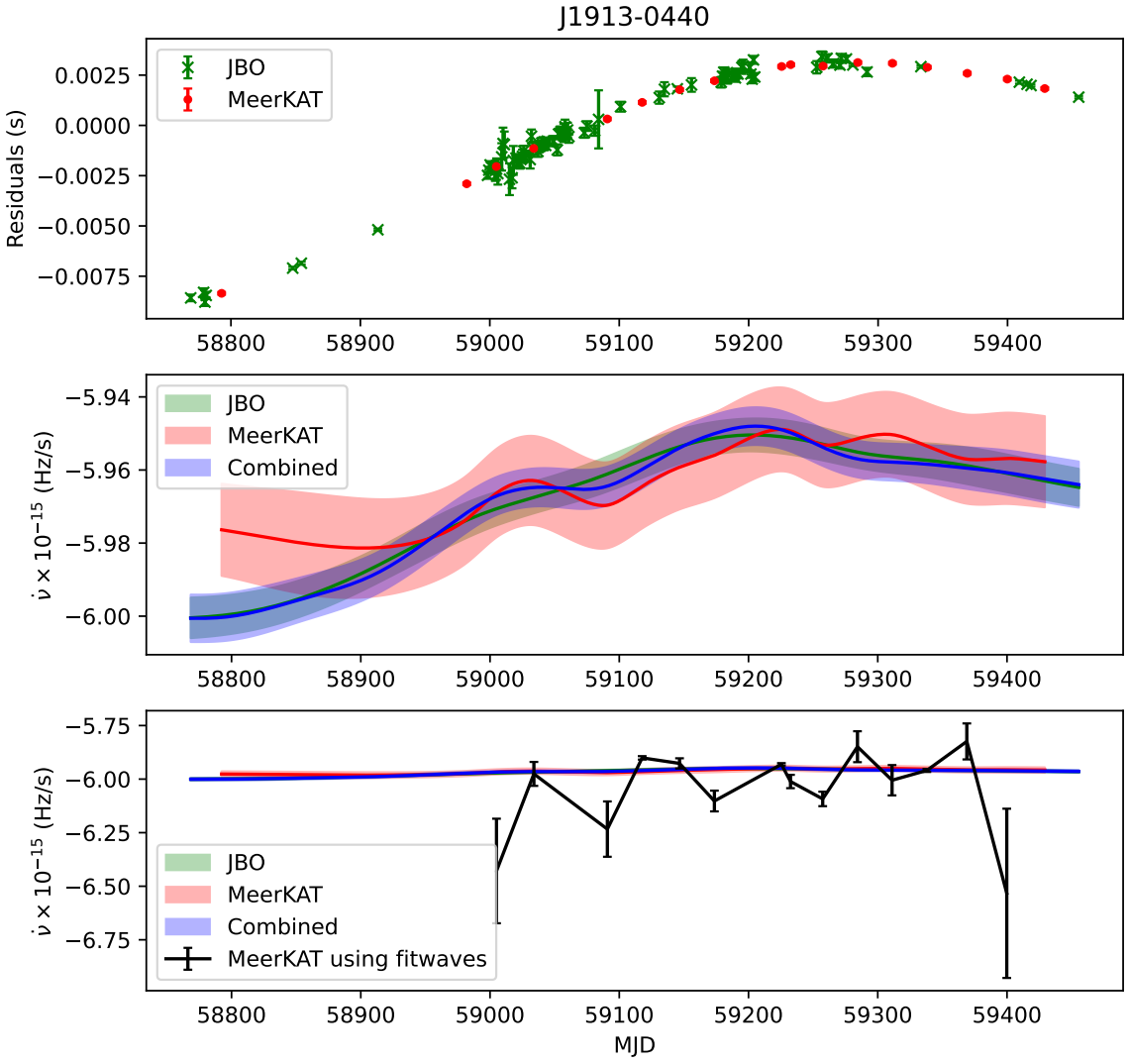

FIGURE 4.8: Timing residuals and $\dot{\nu}$ variations in PSR J1913-0440 using Bayesian and Fitwaves analysis

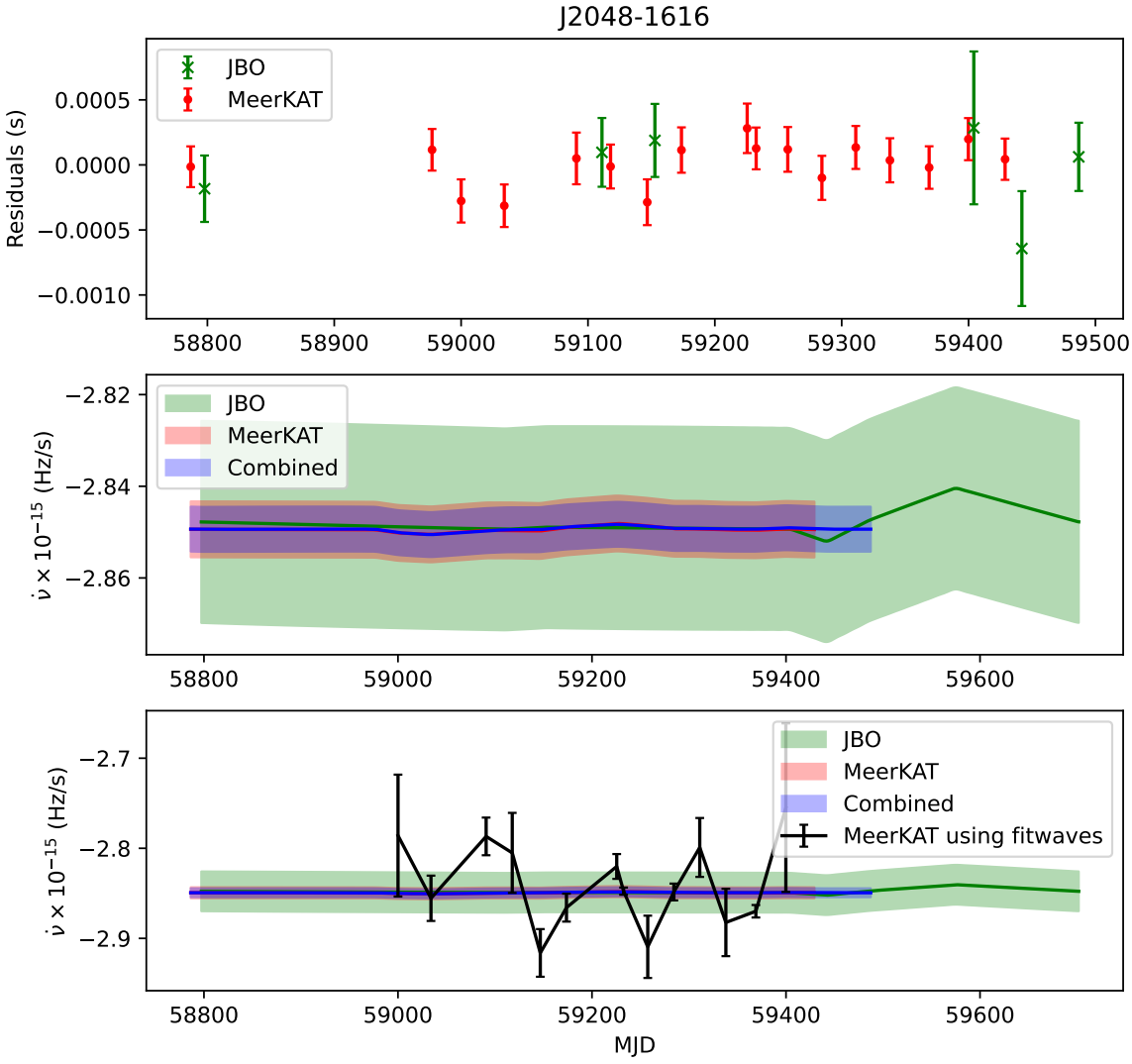

FIGURE 4.9: Timing residuals and $\dot{\nu}$ variations in PSR J2048-1616 using Bayesian and Fitwaves analysis

Chapter 5

Discussions and Conclusions

5.1 Discussions

The fluctuations in the spin-down rate ($\dot{\nu}$) of pulsars may arise from the rearrangement of plasma within the pulsar magnetosphere, as suggested by Shaw et al. (2022). However, this investigation focuses on the significance of employing Bayesian inference to identify the variations in $\dot{\nu}$. Additionally, we examine the consequences of combining datasets from diverse telescopes, aiming to enhance the scope of the data used for analysis. Emphasis is also placed on the pivotal role played by the quality of the combined data in ensuring the robustness of the findings.

For PSRs J1801-2920, J1833-0338, J1901+0331, J1945-0040, J1834-0426, and J1841+0912, the results obtained from fitwave analysis were consistent with Bayesian analysis. However, all three datasets were not effective in estimating $\dot{\nu}$ variations.

In the cases of PSRs J1833-0338 and J1913-0440, combining JBO and MeerKAT data proved beneficial in constraining $\dot{\nu}$ variations. In other instances, either one of the datasets had limited observations, or the timing residuals exhibited significant uncertainty. In such scenarios, it was more prudent to exclude the less informative dataset and combine only with the more reliable one. In the case of PSR J1901+0331, combining both JBO and MeerKAT data facilitated the detection of a decrease in spin-down rate, which was not evident in JBO data alone.

For PSR J1913-0440 and PSR J2048-1616, the elevated uncertainties present in the timing residuals have hindered the execution of the Fitwaves analysis.

5.2 Conclusions

Using the TEMPO2 package, we have computed post-fit residuals for 179 pulsars and presented the updated ephemerides in Table 4.1.

Among these pulsars, we evaluated the variations in $\dot{\nu}$ for 8 pulsars using two distinct methodologies: Bayesian inference and fitwaves analysis. Each analysis utilized three different datasets for every pulsar: 1) Data from the Jodrell Bank Observatory (JBO), 2) Data from the MeerKAT interferometer, and 3) A consolidated dataset containing both JBO and MeerKAT observations. Given that the fitwaves method performs optimally with regularly sampled data, we exclusively employed MeerKAT observations for this analysis. In contrast, Bayesian analysis incorporated all three datasets.

The Fitwaves analysis produced suboptimal outcomes when timing residuals exhibited near-white characteristics or when data was irregularly sampled. In contrast, the Bayesian analysis technique demonstrated effectiveness with every dataset mentioned, including cases with irregular sampling. In conclusion, the Bayesian analysis approach proves versatile, accommodating various types of data, including those with irregular sampling patterns. The study further confirms that combining datasets from different telescopes for analyzing $\dot{\nu}$ variations is proven useful. However, caution is warranted when dealing with datasets featuring high uncertainties, as they can adversely affect study outcomes. Consequently, it is advisable to exclude such data prior to analysis.

Given the pilot nature of this study, the analysis was conducted on a limited set of eight pulsars. Future research endeavors could expand the scope by including a larger set of pulsars, employing different selection criteria. This would allow for an exploration of the impact of combining datasets and employing the Bayesian approach in $\dot{\nu}$ variation studies on a broader scale.

Bibliography

Bailes M., Lyne A. G., Shemar S. L., 1993, in Phillips J. A., Thorsett S. E., Kulkarni S. R., eds, Astronomical Society of the Pacific Conference Series Vol. 36, Planets Around Pulsars. pp 19–30

Bailes M., et al., 2020, Publications of the Astron. Soc. of Australia, 37, e028

Basu A., et al., 2021, Monthly Notices of the Royal Astronomical Society, 510, 4049–4062

Bates S. D., Lorimer D. R., Verbiest J. P. W., 2013, Monthly Notices of the Royal Astronomical Society, 431, 1352

Becker W., Kramer M., Sesana A., 2018, Space Science Reviews, 214

Brook P. R., Karastergiou A., Buchner S., Roberts S. J., Keith M. J., Johnston S., Shannon R. M., 2013, The Astrophysical Journal Letters, 780, L31

Brook P. R., Karastergiou A., Johnston S., Kerr M., Shannon R. M., Roberts S. J., 2015, Monthly Notices of the Royal Astronomical Society, 456, 1374

Edwards R. T., Hobbs G. B., Manchester R. N., 2006, Monthly Notices of the Royal Astronomical Society, 372, 1549

Foreman-Mackey D., Hogg D. W., Lang D., Goodman J., 2013, Publications of the Astronomical Society of the Pacific, 125, 306

Foster R. S., Cordes J. M., 1990, Astrophysical Journal, 364, 123

Han J. L., Manchester R. N., van Straten W., Demorest P., 2018, The Astrophysical Journal Supplement Series, 234, 11

Hankins T. H., Rickett B. J., 1975, Methods in Computational Physics, 14, 55

Hobbs G., Lyne A. G., Kramer M., Martin C. E., Jordan C., 2004, Monthly Notices of the RAS, 353, 1311

Hobbs G. B., Edwards R. T., Manchester R. N., 2006, Monthly Notices of the Royal Astronomical Society, 369, 655

Hobbs G., Lyne A. G., Kramer M., 2010, Monthly Notices of the RAS, 402, 1027

Hotan A. W., van Straten W., Manchester R. N., 2004, Publications of the Astron. Soc. of Australia, 21, 302

Johnston S., et al., 2020, Monthly Notices of the RAS, 493, 3608

Keith M. J., Niţu I. C., 2023, Monthly Notices of the Royal Astronomical Society

Keith M. J., Niţu I. C., Liu Y., 2022, run_enterprise, doi:10.5281/zenodo.5914351, https://doi.org/10.5281/zenodo.5914351

Lentati L., Alexander P., Hobson M. P., Taylor S., Gair J., Balan S. T., van Haasteren R., 2013a, Physical Review D, 87

Lentati L., Alexander P., Hobson M. P., Feroz F., van Haasteren R., Lee K. J., Shannon R. M., 2013b, Monthly Notices of the Royal Astronomical Society, 437, 3004–3023

Lorimer D. R., Kramer M., 2004, Handbook of Pulsar Astronomy. Vol. 4

Lyne A. G., Shemar S. L., Graham Smith F., 2000, Monthly Notices of the Royal Astronomical Society, 315, 534

Lyne A., Hobbs G., Kramer M., Stairs I., Stappers B., 2010, Science, 329, 408–412

Manchester R. N., et al., 2013, Publications of the Astron. Soc. of Australia, 30, e017

Niţ u I. C., Keith M. J., Stappers B. W., Lyne A. G., Mickaliger M. B., 2022, Monthly Notices of the Royal Astronomical Society, 512, 2446

Posselt B., et al., 2021, Monthly Notices of the Royal Astronomical Society

Shannon R. M., Cordes J. M., 2010, The Astrophysical Journal, 725, 1607–1619

Shaw B., et al., 2022, Monthly Notices of the Royal Astronomical Society, 513, 5861–5880

Shemar S. L., Lyne A. G., 1996, Monthly Notices of the RAS, 282, 677

Song X., et al., 2021, Monthly Notices of the RAS, 505, 4456

Song X., et al., 2023, Monthly Notices of the Royal Astronomical Society, 520, 4562

Stairs I. H., Lyne A. G., Shemar S. L., 2000, Nature, 406, 484–486

Taylor J. H., 1992, Philosophical Transactions of the Royal Society of London Series A, 341, 117

Thorsett S. E., Phillips J. A., Cordes J. M., 1993, in Phillips J. A., Thorsett S. E., Kulkarni S. R., eds, Astronomical Society of the Pacific Conference Series Vol. 36, Planets Around Pulsars. pp 31–39

Vigeland S. J., Vallisneri M., 2014, Monthly Notices of the Royal Astronomical Society, 440, 1446–1457

van Straten W., Demorest P., Osłowski S., 2012, Pulsar data analysis with PSRCHIVE (arXiv:1205.6276)